Journal of Volcanology and Geothermal Research 355 (2018) 149–164

Contents lists available at ScienceDirect

Journal of Volcanology and Geothermal Research

journal homepage: www.elsevier.com/locate/jvolgeores

Elemental and Sr-Nd-Pb isotope geochemistry of the Florianópolis Dyke Swarm (Paraná Magmatic Province): crustal contamination and mantle source constraints

Marques L.S. [a,*], De Min A. [b], Rocha-Júnior E.R.V. [c], Babinski M. [d], Bellieni G. [e], Figueiredo A.M.G. [f]

[a] Universidade de São Paulo, Instituto de Astronomia, Geofísica e Ciências Atmosféricas, Rua do Matão, 1226, CEP 05508-090 São Paulo, Brazil
[b] Dipartimento di Matematica e Geoscienze, Università di Trieste, Via E. Weiss, 8, 34127 Trieste, Italy
[c] Departamento de Física da Terra e do Meio Ambiente, Instituto de Física, Universidade Federal da Bahia, Salvador CEP 40170-115, Bahia, Brazil
[d] Universidade de São Paulo, Instituto de Geociências, Centro de Pesquisas Geocronológicas, Rua do Lago, 562, CEP 05508-080 São Paulo, Brazil
[e] Dipartimento di Geoscienze, Università di Padova – retired, Via G. Gradenigo, 6, 35100 Padova, Italy
[f] Instituto de Pesquisas Energéticas e Nucleares, Av. Prof. Lineu Prestes 2242, São Paulo, São Paulo CEP 05508-000, Brazil

ARTICLE INFO

Article history:
Received 30 October 2016
Received in revised form 29 June 2017
Accepted 11 July 2017
Available online 26 July 2017

Keywords:
Florianópolis Dyke Swarm
Paraná Magmatic Province
Mafic dyke swarms
Continental flood basalts
Crustal contamination
Mantle sources

ABSTRACT

The Florianópolis Dyke Swarm is located in Santa Catarina Island, comprising also the adjacent continental area, and belongs to the Paraná Magmatic Province (PMP). The dyke outcrops in the island are 0.1–70 m thick and most of them are coast-parallel (NE-SW trending), with subordinate NW-SE trending. The vast majority of the dykes has SiO_2 varying from 50 to 55 wt% and relatively high-Ti ($TiO_2 > 3$ wt%) contents and these rocks were divided using the criteria commonly used to distinguish the different magma-types identified in the volcanic rocks from the PMP. The Urubici dykes (Sr > 550 μg/g) are the most abundant and some of them experienced crustal contamination reaching to 10%, as evidenced by low P_2O_5/K_2O (0.30–0.21), high $(Rb/Ba)_{PM}$ (1.0–2.2), and radiogenic Sr and Pb isotope compositions ($^{87}Sr/^{86}Sr_i$ up to 0.70716 (back to 125 Ma) and $^{206}Pb/^{204}Pb_m$ up to 19.093). The Pitanga (Sr < 550 μg/g) and the basaltic trachyandesite dykes are less abundant and almost all of them were also substantially affected by at least 15% of crustal assimilation, evidenced by high $(Rb/Ba)_{PM}$ (up to 2.6) and Sr ($^{87}Sr/^{86}Sr_i = 0.70737–0.71758$) and Pb ($^{206}Pb/^{204}Pb_m = 18.446–19.441$) isotope ratios, as well as low P_2O_5/K_2O values (0.30–0.18). The low-Ti ($TiO_2 < 2$ wt%) dykes are scarce and show a large compositional variability (SiO_2: 50.4–64.5 wt%), with similar geochemical characteristics of the low-Ti volcanic rocks (Gramado-Palmas) from southern PMP, although the most primitive dykes show hybrid characteristics of Ribeira and Esmeralda magmas. The presence of granitic xenoliths with border reactions and dykes with diffuse contacts indicate that crustal contamination probably occurred by assimilation from re-melted the host rocks. Considering only the high-Ti Urubici dykes that were not affected by crustal contamination, the Sr, Nd and Pb isotope mixing modelling indicates the participation of a heterogeneous metasomatized (refertilized) subcontinental lithospheric mantle (SCLM). This mantle source was originated by partial melting of a depleted sublithospheric mantle (DMM – Depleted Mantle MORB), which was hybridized by addition of pyroxenite (<5%) and carbonatite (up to 2%) melts. The isotope mixing modelling also points to a significant participation (up to 50%) of Archean SCLM, not evidenced in the mantle sources of the northern PMP high-Ti Pitanga flows (dominated by Neoproterozoic SCLM).

1. Introduction

The origin and evolution of large igneous provinces are widely investigated subjects in the recent years in order to unravel the geodynamic processes, which cause the production of massive volumes of igneous rocks in few million years (Coffin and Eldholm, 1994; Bryan and Ernst, 2008; Ernst, 2014). On continents these provinces are generally constituted by widespread flood basalts and related intrusives (dyke swarms and sills), sporadically accompanied by acid volcanics (e.g., Self et al., 1997).

Many studies have been conducted about the origin and evolution of these huge igneous events, but their origin remains a subject of controversy. Since these igneous manifestations take place away from plate boundaries, they have been explained in terms of hotspot theory. On the one hand, the explanations for origin of hotspots are related with plume/superplume activity, which invokes columnar upwellings originating from the lowermost mantle (e.g., Richards et al., 1989; White

* Corresponding author.
E-mail addresses: leila.marques@iag.usp.br (L.S. Marques), demin@units.it (A. De Min), eduardo.junior@ufba.br (E.R.V. Rocha-Júnior), babinski@usp.br (M. Babinski), giuliano.bellieni@unipd.it (G. Bellieni), anamaria@ipen.br (A.M.G. Figueiredo).

http://dx.doi.org/10.1016/j.jvolgeores.2017.07.005
0377-0273/

and McKenzie, 1989; He et al., 2014, Hoernle et al., 2015). Alternatively, their origin could be more directly linked to heterogeneous sources present either in the subcontinental lithospheric mantle (e.g., De Min et al., 2003; Lustrino, 2005; Merle et al., 2011) or in the shallow mantle (e.g., Anderson, 1994; Anderson, 2005; Coltice et al., 2007).

In this framework, the Paraná-Etendeka continental flood basalts have great importance since they compose one of the largest igneous province of the world, being emplaced about 10 Ma prior to the Western Gondwana breakup and opening Southern Atlantic Ocean. The area affected by this huge magmatism is concentrated in southern Brazil, encompassing also parts of Paraguay, Uruguay and Argentina, constituting the Paraná Magmatic Province (PMP; Fig. 1). In Namibia (the African counterpart) the area covered by the volcanic rocks are significantly smaller compared to those of South America, corresponding to about 10% in volume.

Although many geological, geochemical and geophysical investigations have been accomplished in PMP, there is not a consensus about the causes and the sources of the magmatism. According to some interpretations, the Tristan da Cunha Plume contributed with heat and matter in the petrogenesis of the tholeiites (Gibson et al., 1999; Milner and le Roex, 1996; Ewart et al., 2004; Valente et al., 2007; Hoernle et al., 2015), whereas other models propose melting of heterogeneous subcontinental lithospheric mantle (SCLM) in order to explain the geochemical characteristics of PMP basalts (Bellieni et al., 1984a; Mantovani et al., 1985; Hawkesworth et al., 1986; Petrini et al., 1987; Piccirillo et al., 1989; Peate et al., 1992; Comin-Chiaramonti et al., 1997; Comin-Chiaramonti et al., 1997; Peate et al., 1999; Marques et al., 1999; Iacumin et al., 2003).

The integration of geological, geochemical and geophysical data of the PMP indicated that Tristan da Cunha plume did not act as the trigger of the magmatism, since the paleomagnetic reconstruction at 133 Ma showed that the location of the province was far from the thermal influence area encompassed by such plume (Ernesto et al., 2002). Additionally, Rocha-Júnior et al. (2012) showed that the Tristan da Cunha

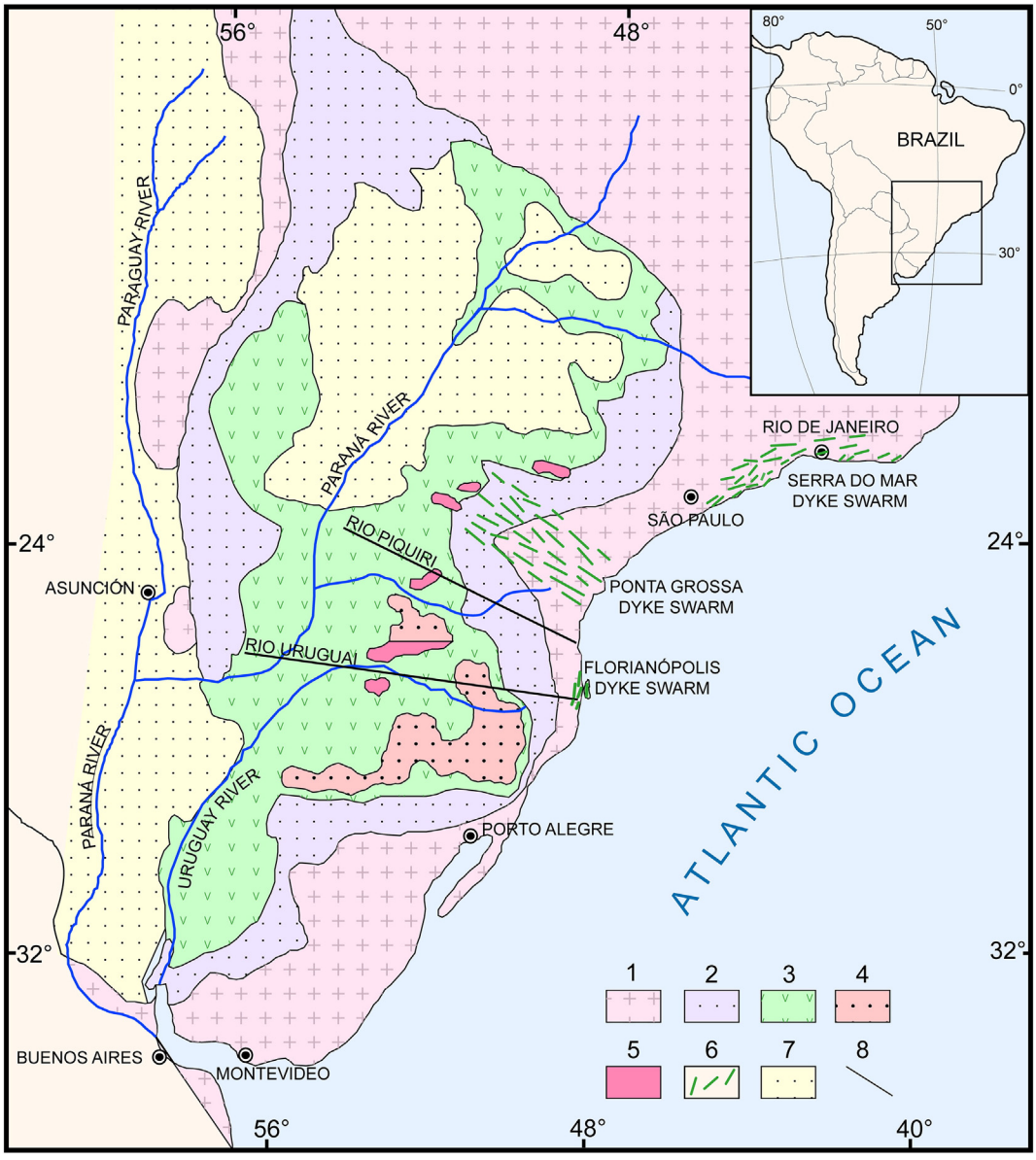

Fig. 1. Generalized geological map of the Paraná Magmatic Province (PMP). 1 = Pre-Devonian basement; 2 = pre-volcanic sedimentary rocks (mainly Paleozoic), including the Botucatu Formation; 3 = flood basalts; 4 = Palmas type acid volcanics; 5 = Chapecó type acid volcanics; 6 = dyke swarms associated with the PMP; 7 = post-volcanic sedimentary rocks (mainly Late Cretaceous); 8 = tectonic and/or magnetic lineaments.
Data sources: Piccirillo and Melfi (1988) and Nardy et al. (2008).

volcanic rocks have suprachondritic osmium isotopic compositions, which are considerably more radiogenic than PMP rocks. These suprachondritic isotope compositions could reflect direct contamination with continental crust (a microcontinent broken off during South Atlantic opening or lower continental crust delamination) in the source of the Tristan da Cunha rocks.

More recently, melting of metasomatized SCLM has been invoked to explain the elemental and isotope (Sr-Nd-Pb-Os) characteristics of the high-Ti tholeiites from PMP (Rosset et al., 2007; Rocha-Júnior et al., 2012, 2013; Comin-Chiaramonti et al., 2014; Marques et al., 2016). The metasomatizing agents could be carbonatite fluids and/or small-volume (pyroxenites) melts related to subduction processes, culminating with those occurred in the Neoproterozoic that resulted in the Western Gondwana assembly (Brasiliano/Pan-African orogeny).

The PMP also encompasses sills mainly concentrated in northern PMP and dyke swarms (Ponta Grossa, Florianópolis, Serra do Mar and Southern Espinhaço). Considering that most of the dykes were emplaced after the main volcanic activity (134–133 Ma; Renne et al., 1992, 1996; Thiede and Vasconcelos, 2010), as pointed out by the integration of paleomagnetic and Ar-Ar geochronological data (Renne et al., 1996; Raposo et al., 1998; Déckart et al., 1998; Rosset et al., 2007), the investigation of these intrusive rocks are crucial for obtaining information about the characteristics of the mantle source involved in the late stages of magmatism.

In order to better constrain the nature of the mantle sources that generated the PMP rocks, new major and trace elements, along with Sr, Nd and Pb isotope data for a suite of samples of the Florianópolis Dyke Swarm (FDS) are presented. This intrusive magmatism is mainly characterized by basic and intermediate tholeiite rocks that crop out at Santa Catarina Island (Fig. 2) and nearby continental coast (Southern Brazil). For this purpose, effects of crustal contamination in the genesis of the dykes were evaluated, since this process occurs frequently during emplacement, being caused by reactions between high temperature mafic magmas with the host rocks, promoting substantial change of the elemental and isotope signatures of the intrusive rocks.

2. The Paraná Magmatic Province

The PMP once covered an area in southern Brazil approximating 1.2×10^6 km^2 with a volume that may have been as great as 7.8×10^5 km^3, overlying the Botucatu Formation sandstones (Jurassic - Early Cretaceous) of the Paraná Basin (Fig. 1; e.g., Piccirillo and Melfi, 1988). The volcanic rocks consist predominantly of a succession of tholeiitic basalts and basaltic andesites, accompanied by subordinated tholeiitic andesites and dacites-rhyolites.

Intrusive rocks, most of them basic in composition are also present, occurring either as sills intruded in sedimentary rocks of the Paraná Basin (Bellieni et al., 1984b; Maniesi and Oliveira, 1997; Ernesto et al., 1999; Machado et al., 2007) or dykes. The latter are concentrated in three swarms, which are referred as Ponta Grossa, Florianópolis, and Serra do Mar (Almeida, 1986; Piccirillo et al., 1990; Garda and Schorscher, 1996; Raposo et al., 1998; Déckart et al., 1998; Marques and Ernesto, 2004; Guedes et al., 2005; Valente et al., 2007; Guedes et al., 2016). Some dykes are also found in the Southern Espinhaço, located at the border of São Francisco Craton (Rosset et al., 2007; Marques et al., 2016).

A considerable number of $^{40}Ar/^{39}Ar$ ages determined in PMP rocks indicates that the main pulse of volcanic activity occurred between 134 and 133 Ma (Renne et al., 1992, 1996; Thiede and Vasconcelos, 2010). The Ponta Grossa dykes intruded mainly in a narrow interval (132–130 Ma; Renne et al., 1996), while for the Serra do Mar Swarm the main phase emplacement varies from 133 to 129 Ma (Déckart et al., 1998), although younger ages (120 Ma) were reported for some dykes located at the coastline by Renne et al. (1993) and older ages (up to 193 Ma) were obtained by Guedes et al. (2005, 2016) nearby Resende town. According to $^{40}Ar/^{39}Ar$ data, the Florianópolis dykes were emplaced in a large time interval, from 131 to 120 Ma (Raposo et al., 1998; Déckart et al., 1998), whereas Florisbal et al. (2014) reported U-Pb (ID-TIMS) ages of 134 Ma determined in baddeleyite/zircon from these dykes.

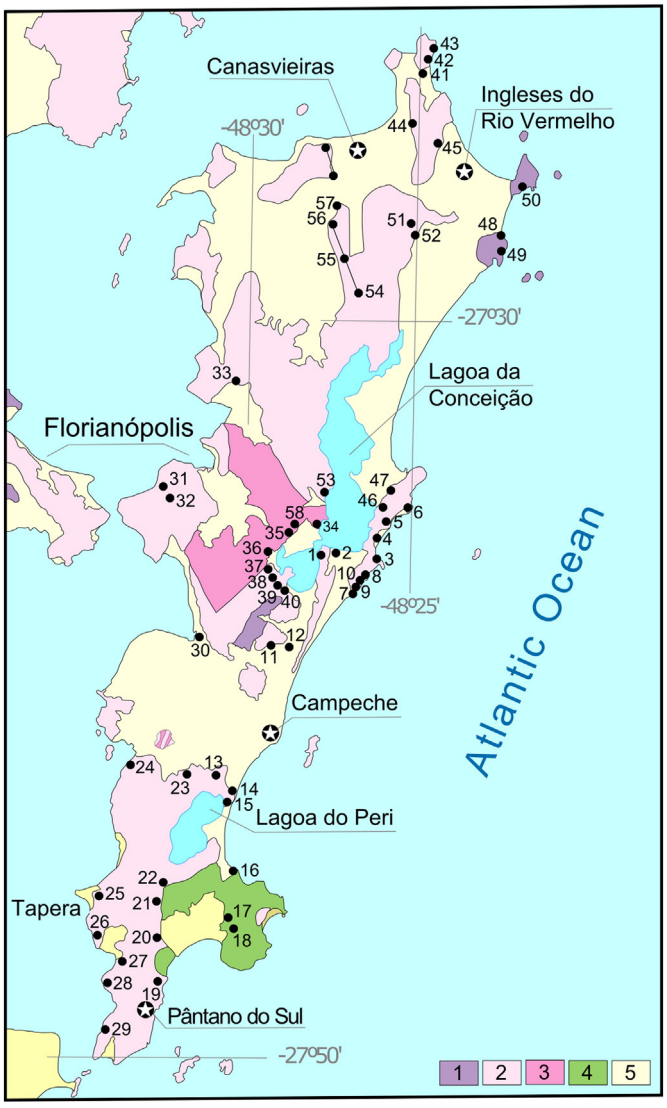

Fig. 2. Geological map of the Santa Catarina Island, showing the locations (site numbers in Table 1 and Supplementary data) of the investigated rocks from the Florianópolis Dyke Swarm, simplified from CPRM (2014). Florianópolis Terrain (1 = granite - gneiss - migmatite rocks of the Águas Mornas Complex); Florianópolis Batholith (2 = Cambirela Rhyolite of the Cambirela Plutonic-Volcanic Suite; 3 = Itacorumbi Granite of the Cambirela Plutonic-Volcanic Suite; 4 = Ilha Granite of the Pedras Grandes Suite); 5 = Cenozoic sedimentary cover.

The basic rocks (extrusive and intrusive) from PMP underwent extensive fractional crystallization (Mg# < 0.56). According to petrographical and geochemical data, and their geographical location, they are divided into two main groups (e.g., Piccirillo and Melfi, 1988; Peate, 1997): (1) Low-Ti tholeiites (Esmeralda and Gramado types), presenting relatively low contents of TiO_2 (≤2 wt%) and incompatible elements (e.g., P, Sr, Ba, Zr, Nb, Ta, Y and LREE) and (2) High-Ti tholeiites (Paranapanema and Pitanga types), containing high TiO_2 concentrations (>2 wt%) and incompatible elements. The high-Ti basalts dominate in northern PMP, whereas the low-Ti basalts are prevalent in southern PMP. Minor volumes of low-Ti (Ribeira type) and high-Ti (Urubici type) basalts occur in northern and southern PMP, respectively.

The acid rocks may also be divided in two main groups with distinct geochemical characteristics (Bellieni et al., 1986; Piccirillo et al., 1987, 1988; Garland et al., 1995; Nardy et al., 2008). The acid volcanics of Chapecó type, which are associated in the field with the Pitanga basalts,

have higher contents of TiO_2, Na_2O, K_2O, P_2O_5 and incompatible trace elements (Sr, Ba, Zr, Hf, Ta and REE) in relation to the Palmas type, genetically related to Esmeralda and Gramado basalts, as well as to the low-Ti tholeiitic andesites.

According to isotope studies, most of the low-Ti volcanic rocks from southern PMP were significantly affected by low-crustal contamination. The initial $^{87}Sr/^{86}Sr$ vary from 0.7046 (Esmeralda), up to 0.7283 in more differentiated rocks (Palmas). The increase of Sr isotope ratios is also accompanied by substantial decrease and increase in Nd and Pb isotope compositions, respectively, reinforcing such petrogenetic processes (Piccirillo and Melfi, 1988; Piccirillo et al., 1989; Garland et al., 1995; Peate and Hawkesworth, 1996; Marques et al., 1989, 1999; Peate, 1997). On the other hand, the high-Ti basalts, as well as the low-Ti Ribeira basalts have initial Sr (0.7054–0.7064), Nd and Pb isotope ratios varying in a narrow interval and evidencing that these rocks did not suffer substantial crustal contamination processes (Mantovani et al., 1985; Petrini et al., 1987; Piccirillo et al., 1989; Marques et al., 1999; Rocha-Júnior et al., 2013). The Chapecó acid rocks have initial Sr isotope ratios from 0.7045 to 0.7079, indicating that some of them suffered crustal contamination, particularly those that crop out to the north of the Piquiri River Lineament (Piccirillo and Melfi, 1988; Garland et al., 1995).

Taking into consideration only the basalts with initial $^{87}Sr/^{86}Sr < 0.7060$, which may be considered as uncontaminated by the continental crust, the incompatible trace element distribution patterns normalized to primordial mantle of Pitanga, Paranapanema and Ribeira basalts are very similar. In contrast, the distribution patterns of Ribeira rocks have significant negative U anomalies, which are not present in the Esmeralda basalts (Marques et al., 1989, 1999; Peate and Hawkesworth, 1996; Peate, 1997; Machado et al., 2015). All southern and northern basalts have negative Ta-Nb anomalies interpreted as the result of mantle metasomatism associated with subducted polygenetic material, which involved the subcontinental lithospheric mantle mainly during Gondwana amalgamation (Neoproterozoic times; Rocha-Júnior et al., 2012, 2013).

In general, the sills and dyke swarms (Ponta Grossa, Serra do Mar, Espinhaço Meridional and Florianópolis) present the same elemental and isotope signatures of the PMP flows and most of them are of high-Ti type (Piccirillo and Melfi, 1988; Piccirillo et al., 1990; Peate, 1997; Guedes et al., 2005, 2016; Valente et al., 2007; Rosset et al., 2007; Marques et al., 2016).

3. The Florianópolis Dyke Swarm

The Florianópolis Dyke Swarm (FDS) is located on Santa Catarina Island, comprising also the adjacent continental area (Fig. 2). There are very few previous studies about these dykes and most of them deal with dating and their relation with the emplacement of PMP flows (Raposo et al., 1998; Déckart et al., 1998; Florisbal et al., 2014). The dykes cut granites originated during the Brasiliano/Pan-African Orogeny, notwithstanding the dykes sometimes cut flow sequences from PMP, as reported by Piccirillo and Melfi (1988), Peate and Hawkesworth (1996).

The crustal section intruded by the FDS dykes belongs to the Dom Feliciano Belt (Southern Brazil and Uruguay), which represents an aggregation of magmatic arcs/continental terranes related to subduction during the Gondwana assembly. The Dom Feliciano Belt trends northeast and in the investigated area (eastern of Santa Catarina State) Archean/Paleoproterozoic supracrustal metamorphic complexes occur along with Neoproterozoic calc-alkaline granites with arc-type signatures (Florisbal et al., 2009 and references therein). In the Santa Catarina Island and nearby coastal area, the dykes intrude mostly granites of the Florianópolis Batholith and the granites-gneisses-migmatites of the Águas Mornas Complex (CPRM, 2014).

The dykes are 0.1 to 70 m thick but most of them have thicknesses between 0.5 and 10 m. They are dark grey to black in color, invariably vertical or sub-vertical and preferably oriented in two directions. The predominant trending is NE-SW (parallel to the coast), coinciding with orientation of the wall rock structures, although NW-SE striking is also found (Raposo et al., 1998; Marques, 2001).

In general, the thicker dykes are characterized by well-developed chilled margins, in straight and sharp contacts with pinkish and greyish host granites, and present progressive increase in the grain size toward their inner parts (Raposo et al., 1998; Marques, 2001). Only few geochemical analyses for FDS rocks are reported in the literature by Peate et al. (1999), Marques (2001) and Florisbal et al. (2014).

The $^{40}Ar/^{39}Ar$ ages applying the ^{40}K decay constants and the age of Fish Canyon, proposed by Renne et al. (2010), vary from 131 to 120 Ma, and are concentrated in two relatively narrow ranges of 131–127 Ma and 123–120 Ma (Raposo et al., 1998; Déckart et al., 1998). According to paleomagnetic results obtained by Raposo et al. (1998), most of the dykes exposed on Santa Catarina Island belong to the youngest magmatic episode. Therefore, the dykes are probably associated with final stages of lithosphere stretching that preceded the oceanic crust formation at the respective latitude. However, Florisbal et al. (2014) reported ages of 134 Ma by using high-precision U-Pb dating in baddeleyite/zircon of dykes exposed on the continental coast, located 90 km south of the Santa Catarina Island. These last ages increase the time interval of dyke emplacement reported by Raposo et al. (1998), indicating that at least some of these intrusive rocks are coeval to the main phase of the PMP. Regarding this aspect, it is important to mention that in the Northwestern Namibia, which was located next to the Florianópolis area in paleogeographic reconstructions, three generations of tholeiitic dykes are found, with $^{39}Ar/^{40}Ar$ ages of 135.2 ± 0.7, 124.1 ± 0.8 Ma and 113.0 ± 0.5 Ma (Will et al., 2016).

4. Analytical procedures

Seventy-three dykes were sampled, resulting in a collection of 108 samples for analysis, since in the thicker dykes two or more samples were collected. Four granite host rocks were also collected and all samples were analyzed for major, minor and some trace elements (Cr, Ni, Ba, Rb, Sr, La, Ce, Nd, Y, Nb and Zr) by X-ray fluorescence at the University of Trieste, Italy, following the procedures described by Rosset et al. (2007). Analytical precision is better than 3% for major element oxides and better than 10% for trace elements.

Sixty-two samples were careful selected for the determination of REE (La, Ce, Nd, Sm, Eu, Tb, Yb, and Lu) and other trace elements (Ta, Th, U, Hf, Sc, and Co) by instrumental neutron activation analysis, which was carried out at the Instituto de Pesquisas Energéticas e Nucleares - CNEN/SP, Brazil. The accuracy and precision are, in general, better than 10% (Figueiredo and Marques, 1989; Marques et al., 1989; Marques, 2001; Rocha-Júnior et al., 2013). The selected samples have small degree of alteration and low values of loss on ignition (in general <2.0 wt%).

Based on major and trace element geochemistry, twenty-three representative FDS samples were selected for the determination of Sr, Nd and Pb isotope ratios. The analyses were performed by thermoionization mass spectrometry at the University of Trieste and Istituto di Geocronologia e Geochimica Isotopica, C.N.R., Pisa (Sr and Nd: Isomas 54E) and at the Centro de Pesquisas Geocronológicas of the Universidade de São Paulo, Brazil (Sr and Nd: Triton mass spectrometer, and Pb: Finnigan MAT 262). The analytical procedures for Sr, Nd and Pb separation is described by Petrini et al. (1987), Babinski et al. (1999), Rocha-Júnior et al. (2013) and references therein. The sample preparation method for the determination of Pb isotopes followed the procedures reported in detail by Marques et al. (1999, 2016).

The Sr isotope ratios were normalized to $^{86}Sr/^{88}Sr = 0.1194$ and replicate analysis for $^{87}Sr/^{86}Sr$ for the NBS987 standard gave a mean value of 0.710238 ± 0.000025 (2σ), with blanks <140 pg. The Nd isotope compositions were normalized to $^{146}Nd/^{144}Nd = 0.7219$, the $^{143}Nd/^{144}Nd$ average for the JNDi-1 standard was 0.512102 ± 0.000003 (2σ) and the analytical blanks were about 50 pg. The blanks during the Pb analyses were about 100 pg and replicate analyses of

the SRM981 NBS standard were used to correct the lead isotope ratios for mass discrimination (0.11%/a.m.u., 0.11%/a.m.u. and 0.07%/a.m.u. for $^{206}Pb/^{204}Pb$, $^{207}Pb/^{204}Pb$ and $^{208}Pb/^{204}Pb$, respectively).

5. Results

The chemical and isotope results of the samples that were analyzed in this investigation are listed in Table 1 and in the Supplementary data, along with the dyke trends and thicknesses. About 80% of the investigated dykes are coast-parallel, trending N30°E–N55°E, which is the same orientation of the Dom Feliciano Belt tectonic features. Approximately 20% of the intrusive rocks trend N15°W–N45°W. The sample location is shown in Fig. 2.

5.1. Classification, nomenclature and magma-types

The vast majority of the FDS intrusions, corresponding to 69 sampled bodies and performing 93% of the intrusions, has SiO_2 contents varying from 50 wt% to 55 wt% and MgO between 5.5 wt% and 3.0 wt%. Three of the remaining dykes have SiO_2 between 55 wt% and 57 wt% and only one is acid in composition, with $SiO_2 = 64$ wt%.

According to the Total Alkalis vs. Silica nomenclature (Le Bas et al., 1986), the rocks are represented by dominant tholeiitic basaltic andesites and subordinate tholeiitic basalts, basaltic trachyandesites, and a rhyodacite (Fig. 3). The basaltic trachyandesites plot on or above the line defined by Irvine and Baragar (1971), which divides the fields of alkaline and sub-alkaline rocks.

The least evolved rocks ($SiO_2 \leq 55$ wt% and MgO > 3 wt%) may be divided in four groups according to their TiO_2 and incompatible trace element distribution (Figs. 4 and 5). The high-Ti dykes are dominant and correspond to the Urubici magma-type ($TiO_2 > 3$ wt%; Sr > 550 μg/g). This magma-type is not voluminous in the PMP, and crop out in the southern PMP and nearby Santa Catarina Island (Piccirillo and Melfi, 1988; Peate, 1997; Peate et al., 1999), although some Mesozoic dykes with similar characteristics also occur in the border of the São Francisco Craton (Rosset et al., 2007; Marques et al., 2016).

There are also minor high-Ti dykes, represented by 9 bodies, which have the same characteristics of the Pitanga magma-type (TiO_2 > 3 wt%; Sr < 550 μg/g). The low-Ti tholeiites ($TiO_2 \leq 2$ wt%) are represented by 3 bodies (tholeiitic basalts) with high Ti/Y (>330), typical of the Ribeira basalts. The low-Ti tholeiitic basaltic andesites and the dacite have the same characteristics of Gramado (Ti/Y < 300) and Palmas volcanic rocks.

Both Urubici and Pitanga dykes are dominated by tholeiitic basaltic andesites, with subordinate tholeiitic basalts and basaltic tachyandesites. Two samples of the tholeiitic basalt group are similar to Pitanga flows, while three the remaining are comparable to Urubici basalts. The basaltic trachyandesites correspond to 5 dykes, which have high-Ti contents and Sr concentrations varying from 368 to 795 μg/g.

Some field relationships are found at Joaquina Beach, where two parallel low-Ti dykes (tholeiitic basalts), trending N45W and with thicknesses of 0.5 m (FL-31) and 2 m (FL-30) crosscut a high-Ti dyke (FL-29; tholeiitic basaltic andesite) of Urubici type, 15 m thick and N15E trending. At the same place, another low-Ti dyke (FL-20; tholeiitic basalt; N55W), crosscuts a high-Ti one (FL-19; tholeiitic basaltic andesite), which trends N20E and is 5 m thick. Therefore, although it is not possible to generalize, there is an indication that low-Ti dykes are younger than those of high-Ti type. It is noteworthy that low-Ti dykes with very similar composition, thickness and trending (NW) to those of Joaquina Beach are also present in the Silveira area (Florisbal et al., 2014), which is located about 90 km south of Santa Catarina Island.

Another crosscutting relationship of two Urubici dykes is found nearby Tapera (southwestern island), where a 0.2 m thick dyke (FL-65; tholeiitic basalt), trending N65E and emplaced in *en echelon* array crosscuts the other one (FL-95; tholeiitic basaltic andesite) trending N45E and 25 m thick.

5.2. Major element behavior

The chemical characteristics of the FDS rocks are similar to those of the volcanic rocks of PMP. The distinction of the different identified groups of rocks is evidenced in Fig. 4 that shows the behavior of major element oxides in relation to MgO, considered as index of magmatic evolution. In general, the contents of SiO_2, FeO_t, Na_2O, K_2O and P_2O_5 increase, whereas those of CaO decrease with differentiation. For the high-Ti dykes, the TiO_2 concentrations tend to increase with evolution degree, especially in the Urubici-like tholeiitic basaltic andesites, except the more evolved dyke (FL-19; $SiO_2 = 55.77$ wt%), which has a significant decrease in titanium content ($TiO_2 = 2.71$ wt%). For the low-Ti dykes, the TiO_2 content is constant for the tholeiitic basalts and tholeiitic basaltic andesites, with a considerable decrease in the dacite.

The Al_2O_3 also has distinct behavior in the high- and low-Ti dykes. For the first group of dykes, an increase of Al_2O_3 concentrations is observed (13 wt% to 15 wt%) for the Pitanga samples and for the basaltic trachyandesites, while for the latter group, the Al_2O_3 decreases with differentiation (from 17 wt% to 13 wt%). Note that the Al_2O_3 is quite spread for the Urubici dykes in relation to MgO.

Only taking into consideration high-Ti dykes, in general, the Pitanga ones have lower contents of TiO_2, K_2O and P_2O_5 in comparison to the Urubici dykes, as also observed for the high-Ti flow analogues of the PMP. The high-Ti dykes belonging to the transitional series, represented by the basaltic trachyandesites, have significantly higher concentrations of Na_2O and K_2O than the tholeiitic basaltic andesites, indicating their slight alkaline tendency. The major elements present some dispersion in the basaltic trachyandesites, but they have slightly lower concentrations of FeO_t and CaO, as well as higher SiO_2 abundances in comparison to most of the high-Ti dykes (Fig. 4). The K_2O content presents a slight decrease with the increase of magmatic evolution, whereas CaO, Al_2O_3 and P_2O_5 have the opposite behavior in these transitional rocks.

5.3. Trace element characteristics

The geochemical differences observed in the oxides of major elements are reinforced by the behavior of incompatible trace elements (Fig. 5). Except for the basaltic trachyandesites, which present some scattering for Rb, Ba, Sr, U and Th, there is a general progressive increase in the concentrations of incompatible trace elements with differentiation. For both the high-Ti Pitanga and Urubici dykes, the Sr contents do not vary significantly with differentiation, whereas a decrease is observed for the low-Ti intrusives, especially in the most differentiated ones (some tholeiitic basaltic andesites with $SiO_2 > 55$ wt% and dacite). Besides the different concentrations of incompatible trace elements of the low- and high-Ti tholeiite dykes, the concentrations of Rb, Ba, Sr, U and Th also allow distinguishing the Urubici, Pitanga and basaltic trachyandesite dykes. The latter ones are characterized by the highest concentrations of Rb, U and Th.

The REE (chondrite normalized; McDonough and Sun, 1995) distribution patterns of the low-Ti FDS rocks are shown in Fig. 6. As the evolution degree increases, a gradual overall enrichment of REE is observed, which is more pronounced for the light REE, generating more fractionated patterns and larger negative Eu anomalies in the differentiated dykes (tholeiitic basalts: $3.7 < (La/Yb)_{CN} < 4.6$; $1.9 < (La/Sm)_{CN} < 2.1$; $0.95 < Eu/Eu^* < 1.11$; tholeiitic basaltic andesites: $3.9 < (La/Yb)_{CN} < 4.6$; $2.4 < (La/Sm)_{CN} < 2.6$; $0.78 < Eu/Eu^* < 0.87$; dacite: $(La/Yb)_{CN} = 6.1$; $(La/Sm)_{CN} = 3.1$; $Eu/Eu^* = 0.82$). It is important to emphasize that positive Eu anomalies, as well as higher concentrations of Al_2O_3 and Sr, observed in the tholeiitic basalts are associated with the presence of abundant millimeter-size plagioclase phenocrysts, generating rocks with porphyritic textures.

The three groups of high-Ti FDS rocks are also distinguished by their REE chondrite normalized distribution patterns (Fig. 7). The Pitanga type dykes have distinctive less fractionated patterns in comparison to the Urubici ones. The $(La/Yb)_{CN}$ of the former group vary from 6.8 to 8.0

Table 1
Whole-rock chemistry and Sr-Nd-Pb isotope compositions of the rocks from the Florianópolis Dyke Swarm.

Sample	FL-12	FL-13	FL-14	FL-16	FL-20	FL-25	FL-28	FL-30	FL-48	FL-56	FL-60	FL-63	FL-65
Site	3	4	5	6	7	9	10	10	12	12	12	14	14
Dyke number	3	4	5	6	9	11	12	14	17	18	19	21	26
Magma-type	Urubici	Urubici	Pitanga	Pitanga	Low-Ti	Urubici	Urubici	Low-Ti	Urubici	Gramado	Urubici	High-Ti	High-Ti
wt%													
SiO_2	53.56	52.12	50.39	53.03	50.68	53.18	53.41	50.42	52.20	55.05	51.36	53.78	50.57
TiO_2	3.91	3.76	3.32	3.12	1.74	4.03	3.46	1.83	4.22	1.79	4.37	3.23	3.86
Al_2O_3	14.43	14.35	13.61	14.32	16.59	14.37	13.93	16.98	14.09	14.09	13.29	14.65	13.72
FeO_t	11.30	12.04	14.81	12.92	11.02	11.63	10.93	10.91	12.52	13.99	13.45	11.07	12.98
MnO	0.15	0.16	0.19	0.20	0.17	0.16	0.15	0.18	0.17	0.22	0.19	0.16	0.18
MgO	3.87	4.75	5.11	4.15	5.47	3.91	5.08	5.21	3.76	2.69	4.20	3.93	4.85
CaO	6.89	7.33	7.61	6.99	10.52	7.23	8.10	10.91	7.51	7.23	8.08	6.07	9.21
Na_2O	3.15	3.14	3.24	3.17	2.92	3.07	2.72	2.81	3.16	3.21	2.57	4.07	2.86
K_2O	2.12	1.72	1.34	1.63	0.72	1.85	1.67	0.56	1.89	1.54	2.05	2.48	1.41
P_2O_5	0.62	0.63	0.38	0.47	0.17	0.57	0.55	0.19	0.48	0.19	0.44	0.56	0.36
Sum	100.00	100.00	100.00	100.00	100.00	100.00	100.00	100.00	100.00	100.00	100.00	100.00	100.00
LOI	1.63	1.91	2.75	2.00	2.29	1.46	1.66	1.61	0.74	0.58	1.62	1.79	1.73
FeO	9.58	8.76	8.65	9.63	6.85	9.66	8.52	7.15	10.85	11.72	9.96	7.55	9.52
Fe_2O_3	1.91	3.64	6.84	3.66	4.63	2.19	2.68	4.18	1.86	2.52	3.88	3.91	3.84
μg/g													
$Cr^{(1)}$	35	32	40	24	146	49	77	136	61	31	69	60	88
$Ni^{(1)}$	46	61	52	29	81	58	66	75	65	33	65	40	78
$Ba^{(1)}$	683	700	288	397	187	687	532	145	649	287	614	722	480
$Rb^{(1)}$	56.0	45.0	68.0	84.0	32.0	39.0	41.0	15.0	37.0	57.0	123.4	80.7	57.7
$Sr^{(1)}$	769	871	454	410	375	721	687	303	740	172	675	529	615
$Zr^{(1)}$	335	220	252	281	141	324	291	150	289	184	323	284	281
$Y^{(1)}$	39	39	49	40	31	39	40	26	37	45	41	36	38
$Nb^{(1)}$	33	28	21	23	12	35	28	12	27	11	31	30	26
$La^{(2)}$	47.5	42.5	30.0	33.2	15.0	47.8	42.7	12.4	48.0	23.6	48.8	50.1	38.3
$Ce^{(2)}$	103	93	62	71	29	104	88	27	98	46	106	104	85
$Nd^{(2)}$	60	54	33	42	16	47	43	18	56	25	55	54	46
$Sm^{(2)}$	11.3	9.9	8.2	8.5	4.4	11.0	9.9	3.9	10.4	6.1	11.4	10.5	9.8
$Eu^{(2)}$	3.71	3.55	2.80	2.60	1.50	3.60	3.16	1.50	3.70	1.70	4.1	3.2	3.5
$Tb^{(2)}$	1.43	1.39	1.39	1.13	0.90	1.52	1.29	0.75	1.54	1.26	1.53	1.37	1.42
$Yb^{(2)}$	2.8	2.3	2.9	3.3	2.2	3.2	2.4	2.2	3.0	3.6	2.3	2.5	2.1
$Lu^{(2)}$	0.37	0.37	0.45	0.41	0.34	0.37	0.35	0.27	0.39	0.70	0.47	0.38	0.35
$Ta^{(2)}$	2.18	2.11	1.23	1.36	0.66	2.43	1.83	0.63	2.25	0.97	2.19	2.16	1.81
$Th^{(2)}$	4.5	4.2	2.93	3.7	1.24	4.6	4.5	1.17	4.6	5.8	4.7	6.5	3.7
$U^{(2)}$	1.00	0.93	0.83	0.84		1.09	0.96	0.40	0.97	1.70	1.05	1.73	0.88
$Hf^{(2)}$	9.7	7.2	5.5	6.4	3.1	9.0	8.7	2.9	7.8	4.6	8.4	7.6	7.1
$Sc^{(2)}$	28.4	29.3	33	34	35	32	27.7	31	29	39	28.8	25.8	29.2
$Co^{(2)}$	37.2	43.1	46	42	40	41	37.6	38.0	40	45	40.3	35.5	40.4
$^{87}Sr/^{86}Sr_m$	0.705455(3)	0.70629(4)	0.70971(2)	0.70911(3)	0.70693(3)	0.70527(3)	0.705895(5)	0.70529(3)	0.705133(6)	0.713673(8)	0.70663(4)	0.708152(4)	0.705625(5)
$^{87}Sr/^{86}Sr_i$	0.705081	0.706030	0.708940	0.708057	0.706491	0.704992	0.705580	0.705048	0.704876	0.711969	0.705690	0.707368	0.705143
$^{143}Nd/^{144}Nd_m$	0.512379(4)	0.512413(5)	0.512468(6)	0.512442(5)		0.512441(6)	0.512380(4)		0.512431(5)	0.512325(4)	0.512406(6)	0.512269(6)	0.512466(6)
$^{143}Nd/^{144}Nd_i$	0.512280	0.512314	0.512369	0.512342		0.512342	0.512273		0.512359	0.512259	0.512327	0.512191	0.512383
$^{206}Pb/^{204}Pb_m$	18.138(26)	18.168(11)	19.441(10)	19.255(18)		18.565(32)	17.659(37)		17.839(61)	18.888(49)	18.683(13)	18.663(7)	18.265(9)
$^{207}Pb/^{204}Pb_m$	15.507(26)	15.548(12)	15.72(10)	15.693(18)		15.609(30)	15.490(43)		15.501(62)	15.662(49)	15.615(14)	15.638(8)	15.581(9)
$^{208}Pb/^{204}Pb_m$	38.396(27)	38.374(12)	39.045(11)	39.482(18)		38.889(29)	38.215(38)		38.222(63)	38.893(51)	38.958(14)	38.937(8)	38.6379(9)

LOI = Loss on Ignition; (1) X Ray Fluorescence; (2) Instrumental Neutron Activation Analysis. The numbers in parenthesis correspond to the uncertainties (2 σ) in the last figures of the measured isotope compositions. The initial isotope ratios were corrected back to 125 Ma, except for those samples dated by $^{40}Ar/^{39}Ar$ (Raposo et al., 1998; Déckart et al., 1998).

Table 1 (*continued*)

Sample	FL-71	FL-81	FL-82	FL-83	FL-84	FL-89	FL-98	FL-102	FL-103	FL-106	FL-110	FL-111	FL-117	FL-120
Site	15	23	24	25	26	29	35	38	39	41	44	45	48	48
Dyke number	27	36	37	38	39	42	48	51	52	54	57	58	61	62
Magma-type	High-Ti	Gramado	Urubici	Palmas	Urubici	Urubici	Urubici	Gramado	Urubici	Urubici	High-Ti	Urubici	Urubici	Urubici
wt%														
SiO_2	53.71	56.06	53.43	64.52	52.74	53.57	52.73	53.27	53.02	53.42	53.78	54.01	52.47	53.31
TiO_2	3.19	1.68	3.91	1.17	3.64	3.51	3.90	1.72	3.15	4.09	3.49	3.91	3.74	3.43
Al_2O_3	14.03	14.21	14.16	13.10	14.46	14.25	14.26	14.89	14.62	13.80	14.33	14.02	13.12	13.37
FeO_t	11.30	13.00	11.40	8.62	11.20	11.44	11.14	13.12	11.05	11.89	11.40	11.31	12.47	11.54
MnO	0.19	0.20	0.14	0.14	0.14	0.16	0.15	0.21	0.14	0.13	0.15	0.15	0.24	0.16
MgO	4.70	3.00	4.44	1.41	5.01	4.26	4.80	3.73	5.29	4.11	4.52	4.27	4.91	4.97
CaO	6.14	6.89	6.99	3.77	7.59	7.51	8.14	8.29	7.53	7.52	5.51	6.89	8.54	7.61
Na_2O	3.78	3.25	2.96	3.89	2.83	3.19	2.83	3.20	3.07	3.00	3.54	2.94	2.81	3.10
K_2O	2.52	1.41	1.91	2.96	1.75	1.68	1.51	1.32	1.69	1.54	2.70	1.95	1.33	1.96
P_2O_5	0.45	0.31	0.66	0.42	0.64	0.43	0.55	0.25	0.44	0.50	0.58	0.55	0.37	0.55
Sum	100.00	100.00	100.00	100.00	100.00	100.00	100.01	100.00	100.00	100.00	100.00	100.00	100.00	100.00
LOI	2.13	1.33	1.73	1.43	1.71	1.16	1.45	1.43	1.94	1.69	2.12	1.21	1.25	1.40
FeO	7.41	11.09	9.85	6.32	9.44	9.27	9.25	10.48	8.53	7.91	8.48	9.59	8.95	8.74
Fe_2O_3	4.32	2.12	1.72	2.56	1.96	2.41	2.10	2.93	2.80	4.42	3.24	1.91	3.91	3.11
µg/g														
$Cr^{(1)}$	63	28	59	1	76	58	113	54	120	43	29	83	59	45
$Ni^{(1)}$	49	32	61	10	73	56	81	43	93	50	55	65	56	48
$Ba^{(1)}$	716	310	691	562	546	574	481	359	585	605	678	606	602	604
$Rb^{(1)}$	150.2	58.9	42.5	121.6	37.0	34.4	25.6	75.4	88.7	31.0	167.0	49.7	43.6	68.3
$Sr^{(1)}$	368	164	731	135	701	633	706	233	642	742	594	611	605	578
$Zr^{(1)}$	304	189	289	292	262	290	248	176	245	344	297	270	281	282
$Y^{(1)}$	36	46	37	61	41	38	35	38	31	45	37	38	40	38
$Nb^{(1)}$	30	11	26	19	23	26	23	12	22	28	24	23	22	23
$La^{(2)}$	52.8	21.8	44.8	44.0	43.0	41.5	36.6	21.8	42.3	48.8	42.4	47.0	38.0	43.0
$Ce^{(2)}$	89	50	101	90	85	92	85	45	81	108	93	100	85	92
$Nd^{(2)}$	51	25	49	45	45	52	44	25	48	55	46	52	46	47
$Sm^{(2)}$	11.3	5.8	10.6	9.0	9.8	10.2	9.8	5.3	9.1	12.0	10.5	9.0	9.5	9.9
$Eu^{(2)}$	3.1	1.70	2.35	2.60	3.5	3.46	3.22	1.70	3.20	3.78	3.48	3.50	2.90	3.40
$Tb^{(2)}$	1.48	1.16	1.45	1.74	1.42	1.29	1.38	1.20	1.15	1.51	1.49	1.56	1.56	1.50
$Yb^{(2)}$	2.2	3.8	2.4	4.9	2.7	2.5	2.5	3.2	2.4	2.9	2.3	2.9	2.7	2.6
$Lu^{(2)}$	0.34	0.63	0.38	0.90	0.42	0.38	0.37	0.60	0.40	0.38	0.38	0.40	0.34	0.39
$Ta^{(2)}$	2.24	0.99	2.08	1.80	1.85	1.85	1.74	0.81	1.70	2.17	2.06	1.90	1.84	1.86
$Th^{(2)}$	6.2	5.4	4.4	12.1	3.9	4.6	3.4	3.8	4.0	4.9	4.7	4.5	3.9	4.1
$U^{(2)}$	1.81	1.67	0.91	2.94	0.91	1.11	0.75	0.85	0.85	1.09	1.13	0.89	0.77	0.94
$Hf^{(2)}$	7.7	4.9	8.3	8.2	7.9	8.4	8.2	4.2	6.1	9.3	9.0	7.3	7.7	7.6
$Sc^{(2)}$	26.9	38	27.5	21	31	25.5	29.4	40	27.0	26.8	27.7	32	31	31
$Co^{(2)}$	36.7	44	37.5	18.2	43	36	39.3	45	40	37.2	37.5	40	37	39
$^{87}Sr/^{86}Sr_m$	0.711147(7)		0.70564(7)		0.705444(8)	0.705438(4)	0.704704(5)		0.707866(6)	0.70575(5)	0.719023(5)	0.706132(7)	0.706657(6)	0.707287(6)
$^{87}Sr/^{86}Sr_i$	0.709049		0.705338		0.705173	0.705159	0.704518		0.707156	0.705535	0.717578	0.705717	0.706289	0.706684
$^{143}Nd/^{144}Nd_m$	0.512271(6)		0.512397(6)		0.512456(4)	0.512379(6)	0.512500(4)		0.512308(5)	0.512388(4)	0.512364(6)	0.512347(4)	0.512383(4)	0.512364(5)
$^{143}Nd/^{144}Nd_i$	0.512181		0.512321		0.512380	0.512302	0.512422		0.512234	0.512305	0.512284	0.512284	0.512305	0.512285
$^{206}Pb/^{204}Pb_m$	19.067(7)		17.834(9)		17.838(39)	17.975(11)	17.909(9)		17.747(25)	19.068(11)	18.522(10)	17.831(28)	19.093(0.09)	18.806(21)
$^{207}Pb/^{204}Pb_m$	15.684(7)		15.529(9)		15.551(39)	15.563(11)	15.536(9)		15.541(26)	15.689(10)	15.596(9)	15.534(27)	15.696(9)	15.658(22)
$^{208}Pb/^{204}Pb_m$	39.303(7)		38.306(9)		38.393(40)	38.508(11)	38.307(9)		38.370(26)	39.558(11)	38.910(9)	38.404(28)	39.103(10)	38.997(22)

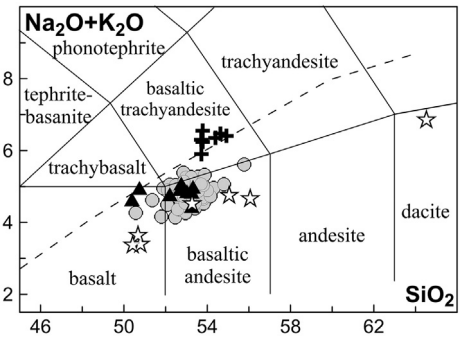

Fig. 3. Total Alkalis (wt%) versus Silica (wt%) nomenclature (Le Bas et al., 1986) of the analyzed rocks from the Florianópolis Dyke Swarm (FDS). Symbols: circles = Urubici type (TiO_2 > 3 wt% and Sr > 550 μg/g), triangles = Pitanga type (TiO_2 > 3 wt% and Sr < 550 μg/g), crosses = basaltic trachyandesites and stars = Low-Ti type (TiO_2 < 2 wt%).

(average = 7.5 ± 0.5; N = 7), and between 8.1 and 14.0 (average = 11 ± 2; N = 40) in the latter. The Pitanga and Urubici dykes have small either positive or negative Eu anomalies, although in most of them the anomalies are slightly positive. For Pitanga intrusives, the Eu/Eu* ratios have small variation and are situated between 0.93 and 1.13 (average = 1.02 ± 0.09; N = 9), whereas for the Urubici dykes this ratio ranges from 0.69 to 1.47 (average = 1.06 ± 0.12; N = 40).

The basaltic trachyandesites tend to be enriched light REE (Fig. 7) in comparison to the other high-Ti dykes, with $(La/Yb)_{CN}$ ratios lying between 10.8 and 15.9 (average = 13 ± 2; N = 7) and presenting both small negative and positive Eu anomalies (0.87 ≤ Eu/Eu* ≤ 1.10; average = 1.01 ± 0.09).

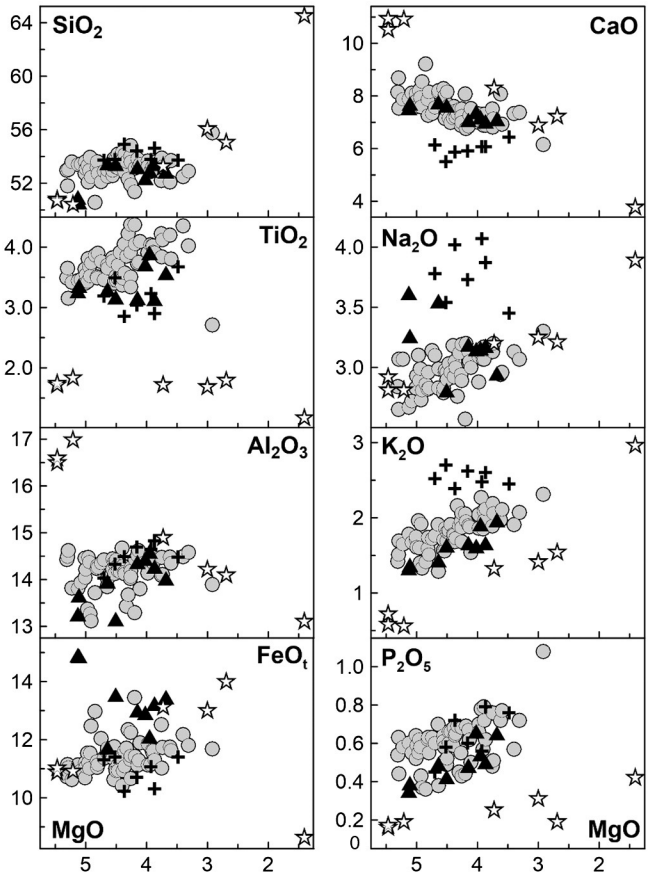

Fig. 4. Major elements (wt%) versus MgO (wt%), considered as a differentiation index, for the rocks from FDS. Symbols as in Fig. 3.

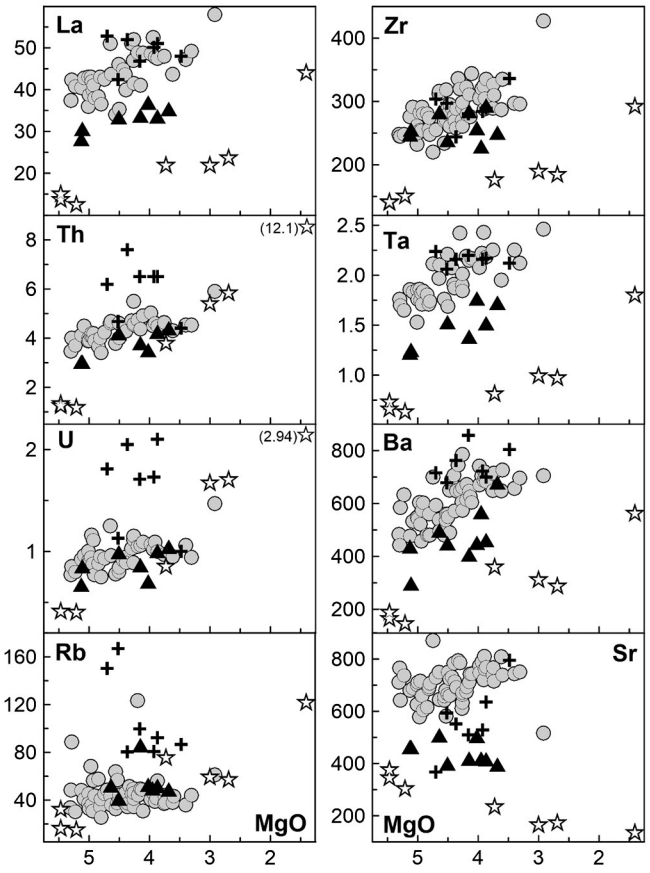

Fig. 5. Trace elements (μg/g) versus MgO (wt%) of the rocks from FDS. Symbols as in Fig. 3.

The primitive mantle normalized (McDonough and Sun, 1995) distribution patterns of trace elements for the low-Ti FDS rocks are shown in Fig. 8. These dykes present a large compositional variation and all are characterized by negative Nb-Ta, Ti and P anomalies, which increase with differentiation. There is also a remarkable variation in the primitive mantle normalized $(Rb/Ba)_{PM}$ ratios, ranging from 1.1 in the least evolved rocks to 2.4 in the differentiated ones. The low-Ti tholeiitic basalts and the more primitive basaltic andesites present slight negative Sr anomalies (related to plagioclase accumulation), whereas the most evolved basaltic andesite and the dacite have notable negative anomalies, indicating fractional crystallization of this mineral during magma evolution. It is noteworthy that the tholeiitic basalts have Ti/Y ratios and some high field strength element (HFSE) concentrations

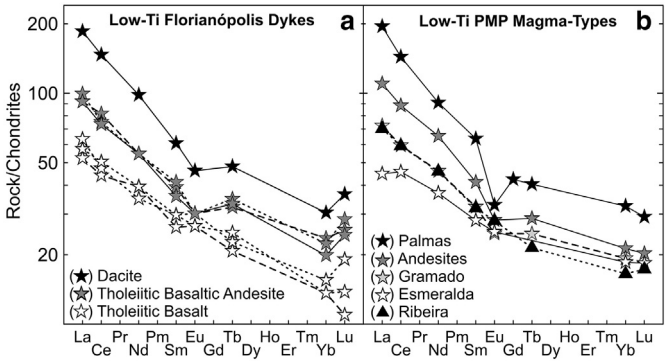

Fig. 6. Rare earth distribution patterns (chondrite normalized; McDonough and Sun, 1995) for the low-Ti dykes from FDS and comparison to the low-Ti volcanic rocks from the Paraná Magmatic Province (PMP).
Data sources: Piccirillo and Melfi (1988); Marques et al. (1989); Peate (1997); Marques et al. (1999); Garland et al. (1995); Machado et al. (2015).

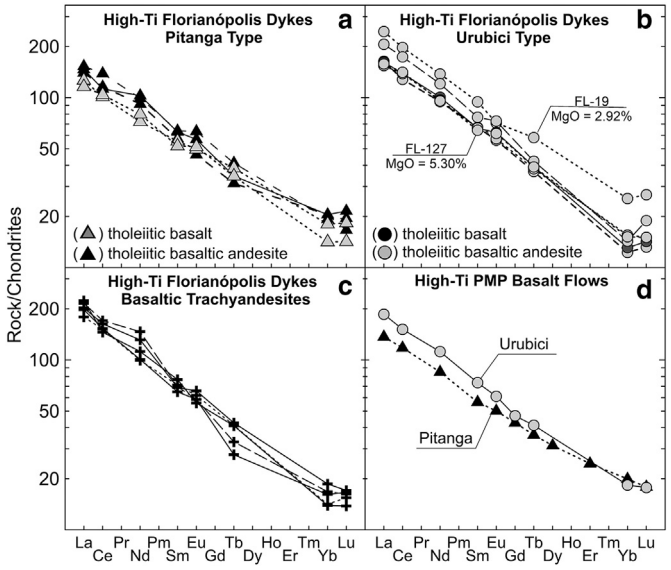

Fig. 7. Rare earth distribution patterns (chondrite normalized; McDonough and Sun, 1995) for the high-Ti dykes from FDS and comparison to the high-Ti volcanic rocks from PMP (Piccirillo and Melfi, 1988; Marques et al., 1989; Peate, 1997; Peate et al., 1999; Marques et al., 1999; Rocha-Júnior et al., 2012, 2013).

(e.g., Ti, Zr, Y) similar to those of the Ribeira flows. However, the distribution patterns of these low-Ti basic dykes exhibit significant negative P and positive Ba anomalies, which typify the Esmeralda and Gramado basalts.

The multi-elemental distribution patterns of the Pitanga and Urubici dykes are in general very similar to the respective effusive analogues, considering the same contents of MgO (Fig. 9). Both groups of intrusive rocks are characterized by significant negative U, Nb-Ta and Sr anomalies. However, it is important to note that some Pitanga dykes present $(Rb/Ba)_{PM}$ ratios reaching up to 2.6, which are significantly larger than those of the Pitanga flows (0.36–0.88). Although the vast majority of Urubici dykes have $(Rb/Ba)_{PM}$ ratios <0.9, in a considerable number of dykes they are larger, with values as high as 2.2. For both Pitanga and Urubici dykes, the high $(Rb/Ba)_{PM}$ ratios are accompanied by low P_2O_5/K_2O values (<0.30).

In general, the primitive mantle normalized distribution patterns of the basaltic thachyandesites with Sr < 550 μg/g are comparable to the Pitanga dykes, except for K contents, which are considerably more enriched in the former. The basaltic thachyandesites containing Sr > 550 μg/g present distribution patterns that resemble those relative to the Urubici dykes, although they have significant enrichment in U and Th (Fig. 9). The basaltic thachyandesites have $(Rb/Ba)_{PM}$, ranging from 1.2 to 2.7, and negative Sr anomalies, which are larger in rocks with higher U and Th concentrations.

5.4. Sr, Nd and Pb isotope compositions

Sr and Nd isotope ratios were age-corrected (hereafter $^{87}Sr/^{86}Sr_i$ and $^{143}Nd/^{144}Nd_i$, respectively) taking into account the ^{40}Ar-^{39}Ar ages reported by Raposo et al. (1998) and Déckart et al. (1998), recalculated applying the ^{40}K decay constants and the Fish Canyon age (Renne et al., 2010). For the samples that were not dated, an estimated age of 125 Ma was used to calculate the initial isotope compositions. It is important to emphasize that both initial Sr and Nd isotope ratios do not change expressively if the age for correction is 134 Ma, which was obtained for dykes outcropping near south of Santa Catarina Island (Florisbal et al., 2009). Present day $^{206}Pb/^{204}Pb_m$, $^{207}Pb/^{204}Pb_m$ and $^{208}Pb/^{204}Pb_m$ are used because the investigated samples were not analyzed for the Pb concentration, as well as most of the PMP rocks reported in the literature.

For three low-Ti dykes Sr isotope compositions were also measured. Two of them correspond to tholeiitic basalts (FL-20 and FL-30) and the other is a tholeiitic basaltic andesite (FL-56). Only the last sample was also analyzed for Nd and Pb isotopes. The most primitive low-Ti dykes have less radiogenic Sr ($^{87}Sr/^{86}Sr_i = 0.70505$ and 0.70649) than the most differentiated tholeiitic basaltic andesite, which is significantly enriched in radiogenic Sr ($^{87}Sr/^{86}Sr_i = 0.71197$) and Pb ($^{206}Pb/^{204}Pb_m = 18.888$; $^{207}Pb/^{204}Pb_m = 15.662$; $^{208}Pb/^{204}Pb_m = 38.893$), and depleted in radiogenic Nd ($^{143}Nd/^{144}Nd_i = 0.51226$). The isotope ratios are in the range of those presented by the low-Ti Esmeralda and Gramado flows from southern PMP (Figs. 10, 11 and 12).

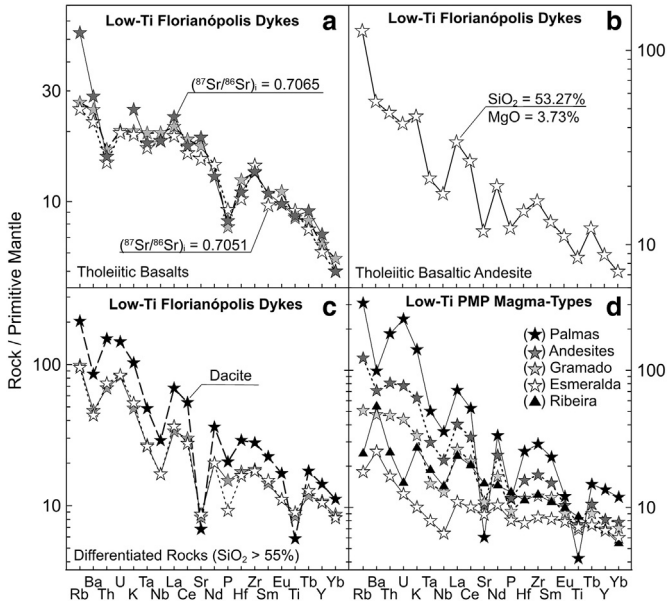

Fig. 8. Trace element distribution patterns normalized to primitive mantle (McDonough and Sun, 1995) for the low-Ti rocks from FDS and comparison to the low-Ti volcanic rocks from PMP (references as in Fig. 6). The differentiated rocks encompass two tholeiitic basaltic andesites and a dacite.

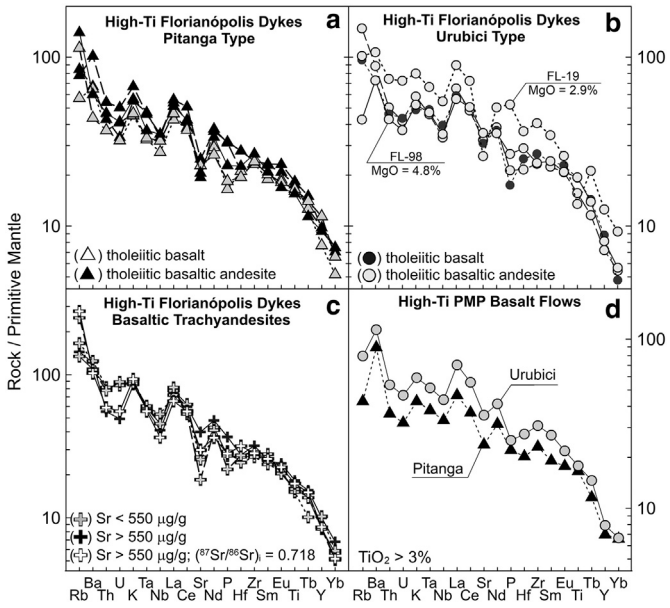

Fig. 9. Trace element distribution patterns normalized to primitive mantle (McDonough and Sun, 1995) for the high-Ti rocks from FDS and comparison to the high-Ti volcanic rocks from PMP (references as in Fig. 7).

The isotope ratios of Sr, Nd and Pb of the two analyzed Pitanga dykes present some variation ($^{87}Sr/^{86}Sr_i$ = 0.70806–0.70894; $^{143}Nd/^{144}Nd_i$ = 0.51234–0.51237; $^{206}Pb/^{204}Pb_m$ = 19.255–19.441). These Sr and Pb isotope ratios are significantly higher than those of the Pitanga flows ($^{87}Sr/^{86}Sr_i = 0.7057 \pm 0.0002$; $^{143}Nd/^{144}Nd_i = 0.51277 \pm 0.00005$; $^{206}Pb/^{204}Pb_m = 17.9 \pm 0.1$), whereas for Nd they are similar (Piccirillo and Melfi, 1988; Peate, 1997; Marques et al., 1999; Rocha-Júnior et al., 2012, 2013). It is noteworthy to mention that the Pitanga dykes have even more radiogenic Sr and Pb isotope ratios than those of the Gramado basalts, which are characterized by extensive low-pressure crustal contamination (Figs. 10, 11 and 12). This petrogenetic process, associated with fractional crystallization, caused substantial compositional variability, especially in incompatible trace elements, as shown in previous studies on the Gramado and Palmas volcanic rocks (e.g., Piccirillo and Melfi, 1988; Peate, 1997; Garland et al., 1995).

Sixteen dykes of Urubici type were analyzed for Sr, Nd and Pb isotopes and the data show large variation, mainly for Sr and Pb ($^{87}Sr/^{86}Sr_i$ = 0.70452–0.70716 with a mean = 0.7056 ± 0.0007; $^{143}Nd/^{144}Nd_i$ = 0.51224–0.51242 with a mean = 0.51232 ± 0.00005; $^{206}Pb/^{204}Pb_m$ = 17.659–19.093 with a mean = 18.2 ± 0.5). Although most of the dykes have isotope compositions similar to those of the Urubici flows (Piccirillo and Melfi, 1988; Peate, 1997; Marques et al., 1999; Peate et al., 1999), the most radiogenic ones are out of the range presented for these volcanic rocks, which are characterized by relatively small variations in the Sr, Nd and Pb isotope ratios ($^{87}Sr/^{86}Sr_i = 0.7053 \pm 0.0004$; $^{143}Nd/^{144}Nd_i = 0.51229 \pm 0.00005$; $^{206}Pb/^{204}Pb_m = 17.7 \pm 0.2$). Note that the sample FL-98 (SiO_2 = 52.73 wt%; MgO = 4.80 wt%) was analyzed by Rocha-Júnior et al. (2012) for Sr ($^{87}Sr/^{86}Sr_i$ = 0.70452), Nd ($^{143}Nd/^{144}Nd_i$ = 0.51242), Pb ($^{206}Pb/^{204}Pb_m$ = 17.909; $^{207}Pb/^{204}Pb_m$ = 15.536; $^{208}Pb/^{204}Pb_m$ = 38.307) and Os ($^{187}Os/^{188}Os_i$ = 0.12631) isotopes.

Regarding the basaltic trachyandesite dykes, four samples were analyzed for Pb isotopes and three of them were also investigated for Sr and Nd isotopes (Figs. 10, 11 and 12). The data show highly radiogenic Sr and Pb compositions and particularly for Sr isotopes there is a large variation ($^{87}Sr/^{86}Sr_i$ = 0.70737–0.71758; $^{143}Nd/^{144}Nd_i$ = 0.51218–0.51229; $^{206}Pb/^{204}Pb_m$ = 18.446–19.067). These dykes have isotope compositions similar to those of the Gramado basalts, but some of them are even more radiogenic in Pb.

Taking into account all the analyzed samples, $^{87}Sr/^{86}Sr_i$ is negatively and positively correlated with P_2O_5/K_2O and $(Rb/Ba)_{PM}$, respectively

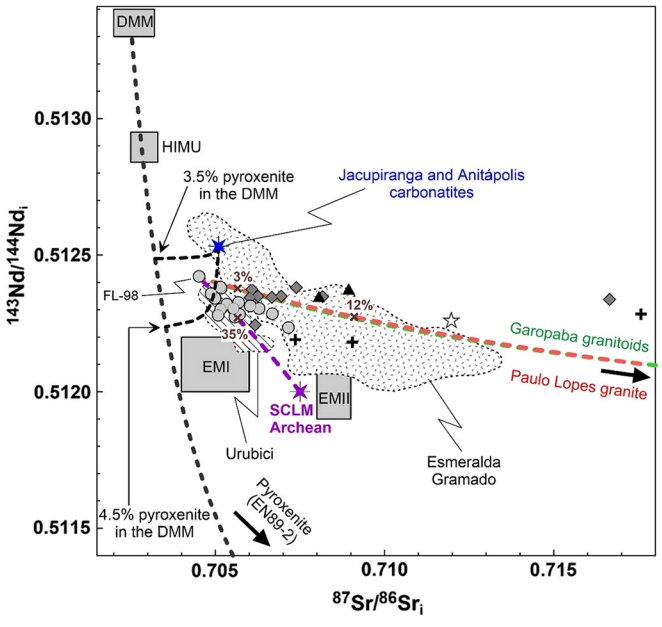

Fig. 10. Initial $^{87}Sr/^{86}Sr$ and $^{143}Nd/^{144}Nd$ isotope ratios of rocks from FDS and basalts from PMP (Piccirillo and Melfi, 1988; Marques et al., 1989; Peate, 1997; Peate et al., 1999; Marques et al., 1999; Rocha-Júnior et al., 2012, 2013). The parameters used in the different mixing modelling are shown in Table 2. Symbols: circles = Urubici type (TiO_2 > 3 wt% and Sr > 550 μg/g), triangles = Pitanga type (TiO_2 > 3 wt% and Sr < 550 μg/g), crosses = basaltic trachyandesites and stars = Low-Ti type (TiO_2 < 2 wt%); diamonds = dykes from FDS published by Florisbal et al. (2009, 2014).

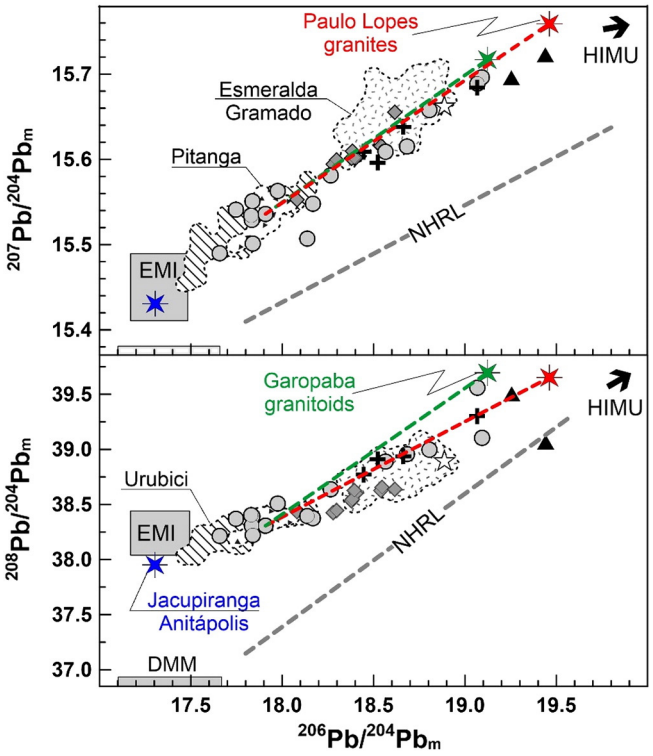

Fig. 11. (a) Measured $^{206}Pb/^{204}Pb$ and $^{207}Pb/^{204}Pb$ and (b) $^{208}Pb/^{204}Pb$ and $^{206}Pb/^{204}Pb$ isotope compositions of rocks from FDS and basalts from PMP (Piccirillo and Melfi, 1988; Marques et al., 1989; Peate, 1997; Peate et al., 1999; Marques et al., 1999; Rocha-Júnior et al., 2012, 2013). Symbols as in Fig. 10. NHRL = Northern Hemisphere Reference Line.

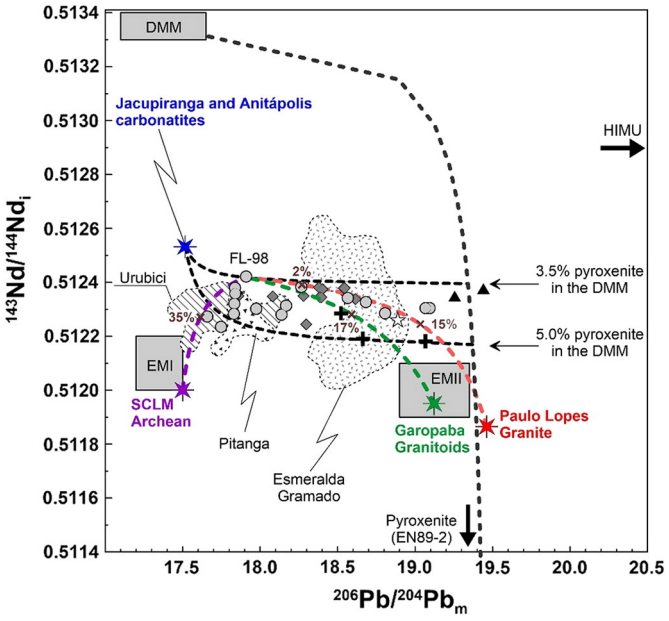

Fig. 12. Plot of initial $^{143}Nd/^{144}Nd$ versus measured $^{206}Pb/^{204}Pb$ of rocks from FDS and basalts from PMP (Piccirillo and Melfi, 1988; Marques et al., 1989; Peate, 1997; Peate et al., 1999; Marques et al., 1999; Rocha-Júnior et al., 2012, 2013). Symbols as in Fig. 10. The parameters used in the different mixing modelling are shown in Table 2.

(Fig. 13). Although these relationships are observed in the Gramado basalts, they have not been verified in the Pitanga and Urubici rocks from the PMP analyzed previously (e.g., Piccirillo and Melfi, 1988; Peate, 1997; Marques et al., 1999, 2016; Peate et al., 1999; Rocha-Júnior et al., 2012, 2013). It is important to note that the latter researchers observed that the high-Ti volcanic rocks were not or very little affected by crustal contamination in their genesis, as indicated by their low initial $^{87}Sr/^{86}Sr$ (<0.7060).

6. Discussion

The Early Cretaceous intrusive magmatism in Santa Catarina Island and adjacent coastal areas comprises predominantly high-Ti and subordinate low-Ti dykes. In general, the contacts of the dykes with the invaded rocks are well-defined, with fine-grained chilled margins, although in some locations they are diffuse, indicating re-melting of the host rocks, as also pointed out by Florisbal et al. (2014) for dyke outcrops in the nearby continental area. The interaction between the magmas and the wall rocks is also evidenced by the presence of border reactions in granitic xenoliths found in some dykes. Since these processes often cause substantial changes in the original chemical and isotope signatures of the magmas, before the discussion about the mantle sources involved in the genesis of the dykes from FDS, it is necessary to investigate the effects of crustal contamination in such rocks.

The FDS rocks were mainly emplaced in the Florianópolis Batholith and most of its granites are characterized by TiO_2 (<0.7 wt%; average = 0.3 ± 0.2 wt%), Ti/Y (<150; average = 57 ± 44), Ti/Zr (<20; average = 9 ± 4), Zr/La (<6.5; average = 4 ± 2), P_2O_5/K_2O (<0.05; average = 0.02 ± 0.01), $(Rb/Ba)_{PM}$ (>1.5; average = 9 ± 10), and La/Tb (>22; average = 53 ± 22), as indicated by the present study (Table 1 and Supplementary data) and by Florisbal et al. (2009). Considering that some of the above chemical parameters are commonly used to distinguish the different basalts from the PMP (e.g., Peate et al., 1992; Peate, 1997), a contamination with such granites could cause misleading in the magma-type classification, changing also other incompatible trace element characteristics of the dykes.

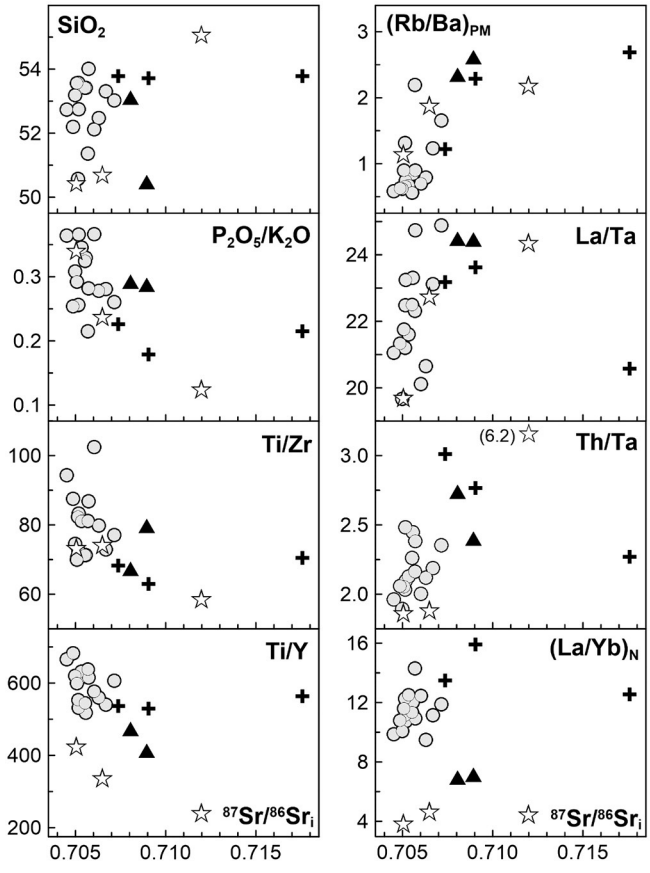

Fig. 13. Major element concentrations (wt%) and trace element ratios versus initial $^{87}Sr/^{86}Sr$ of dykes from FDS. Symbols as in Fig. 3.

6.1. The low-Ti dykes

The low-Ti dykes are very few and have a large compositional variability (SiO_2: 50.4–64.5 wt%; MgO: 5.5–1.4 wt%). The behavior of major and trace element in variation diagrams, in conjunction with REE and multi-elemental distribution patterns are very close to those of low-Ti volcanic series from southern PMP, suggesting similar petrogenesis (Figs. 4, 5, 6 and 8). Thus, it may be concluded that the magmatic evolution of the low-Ti dykes was probably dominated by fractional crystallization process, mainly controlled by plagioclase, clinopyroxene and magnetite, associated with significant crustal contamination, as proposed in previous studies of the PMP (Piccirillo and Melfi, 1988; Piccirillo et al., 1989; Peate and Hawkesworth, 1996; Peate, 1997; Garland et al., 1995; Barreto et al., 2016).

Evidence of crustal contamination was found in the petrogenesis of the low-Ti (basaltic andesites) dykes, since these rocks have radiogenic Sr and Pb, and non-radiogenic Nd isotope ratios (FL-56; $^{87}Sr/^{86}Sr_i$ = 0.71197; $^{206}Pb/^{204}Pb_m$ = 18.888, $^{143}Nd/^{144}Nd_i$ = 0.51259). It is important to remark that the FL-30 tholeiitic basalt has the highest P_2O_5/K_2O (0.34) and the lowest $^{87}Sr/^{86}Sr_i$ (0.70505) and $(Rb/Ba)_{PM}$ (1.1) ratios. The later ratio is comparable to those of Esmeralda (0.62–1.27; average = 0.9 ± 0.3) basalts, but it is significantly higher than those of Ribeira (0.36–0.88; average = 0.6 ± 0.2) tholeiites (Piccirillo and Melfi, 1988; Peate, 1997; Marques et al., 1999; Machado et al., 2015). In comparison to FL-30, the other tholeiitic basalt (FL-20) is enriched in radiogenic Sr ($^{87}Sr/^{86}Sr_i$ = 0.70649) and in incompatible trace elements (REE, Th, Ta, Hf, Ba and Rb), for similar SiO_2 and MgO contents (Figs. 4, 5, 6, 8 and 13), demonstrating the effect of crustal contamination. It is important to note that the most primitive low-Ti dykes (tholeiitic basalts sampled at Joaquina Beach) have hybrid characteristics of Ribeira and Esmeralda-Gramado basalts. This suggests that the Esmeralda-Gramado dykes may have experienced a very small assimilation of the Urubici ones, probably during their emplacement, since the former crosscut the later, generating a minimal enrichment of some trace elements, such as the HFSE.

The evolution of low-Ti rocks by assimilation and fractional crystallization processes increased the concentrations of incompatible trace elements, especially those elements highly concentrated in the granitic country rocks, such as light REE, Rb, Th and U. This process caused progressively increasing of $(Rb/Ba)_{PM}$, La/Tb, U/Th, La/Ta, Th/Ta and Zr/Th ratios, which are larger than those expected for differentiation in a closed system.

6.2. Crustal contamination effects on the high-Ti dykes

The high-Ti dykes were divided into three groups according to major and trace elemental geochemistry. The Urubici dykes are by far the most abundant rocks from the FDS and have the same compositional variability observed for the flows, presenting MgO varying from 5.31 wt% to 2.95 wt%, although a considerable number of dykes has MgO < 4 wt%. The REE distribution patterns of the least differentiated Urubici dykes are very similar to the flow analogues (Fig. 7). While an overall enrichment of REE with the differentiation is observed, there is no clear correlation between $(La/Yb)_N$ and Eu/Eu* with either MgO or SiO_2 contents. However, the REE patterns tend to be more fractionated, as evidenced by the $(La/Yb)_N$ ratios, with increasing of $^{87}Sr/^{86}Sr_i$, showing the role of crustal contamination in these rocks (Fig. 13).

The primitive mantle normalized distribution patterns of incompatible trace elements of some Urubici dykes are distinct with respect to the flows, especially concerning the Rb enrichment in relation to Ba

(Fig. 9). Although some scatter exist, there is an increase of SiO_2, $(Rb/Ba)_{PM}$, Th/Ta and La/Ta and a decrease of P_2O_5/K_2O, Ti/Zr and Ti/Y with the increase of $^{87}Sr/^{86}Sr_i$ (Fig. 13). Remarkably, the more differentiated dykes (MgO < 4 wt%) have $^{87}Sr/^{86}Sr_i < 0.7060$, indicating that the most primitive magmas, probably due to their higher temperatures, interacted to a larger extent with the granitic wall rocks.

The Pitanga dykes have a moderate variation in MgO contents (5.1–3.7 wt%) and for similar contents of this oxide, the dykes are slightly enriched in light REE and other highly incompatible trace elements (U, Th, Ta, Nb) in comparison to the Pitanga flows (Figs. 7 and 9). As also noted for the Urubici dykes, a significant number of the Pitanga dykes does not show a positive Ba anomaly with respect to Rb and Th, an important feature of the flow analogues, in the multi-elemental distribution patterns normalized to the primitive mantle, presenting high $(Rb/Ba)_{PM}$, which reaches up to 2.6. It is noteworthy that the two highest values of $(Rb/Ba)_{PM}$ (>2) correspond to the Pitanga dykes with highly radiogenic Sr and Pb isotope ratios (Figs. 9, 10, 11 and 13), whose values are even larger than those observed for the Urubici contaminated dykes. Therefore, some Pitanga dykes have undergone higher extents of crustal contamination in comparison to those of the Urubici ones, with significant modification of their original geochemical signatures.

Regarding the basaltic trachyandesites, although they have higher contents of K_2O, the other elemental and isotope characteristics tend to be similar to the Pitanga or to Urubici dykes, especially those having $(Rb/Ba)_{PM} > 1$. The basaltic trachyandesites are characterized by very radiogenic isotope compositions, with $^{87}Sr/^{86}Sr_i$ as high as 0.71758 (Figs. 9, 10 and 13), evidencing the occurrence of a considerable crustal contamination process.

Supposing that the felsic contaminant had a composition similar to the granites that belong to the Florianópolis Batholith (present study and Florisbal et al., 2009), the interaction with the original magmas, would cause a decrease of P_2O_5/K_2O and an increase in the $(Rb/Ba)_{PM}$, as observed for some Pitanga and basaltic trachyandesite dykes. Considering a simple mixing process between a typical Urubici magma type (SiO_2 = 50 wt%, K_2O = 1.5 wt% and P_2O_5 = 0.5 wt%) and the wall rocks (SiO_2 = 75 wt%, K_2O = 5 wt% and P_2O_5 = 0.1 wt%), an assimilation of about 10–15% of the felsic rocks would significantly decrease P_2O_5/K_2O (from 0.35 to 0.17) and increase the SiO_2 content (reaching 53–54 wt%), as observed for the most contaminated Urubici dykes (Fig. 13). Even more importantly, there would also be a decrease of TiO_2 and Sr, which are the parameters commonly used to distinguish between Pitanga and Urubici magma types. Consequently, it is possible that a significant contamination of original Urubici magmas would generate rocks presenting the observed features of some Pitanga and basaltic trachyandesite dykes, such as high $(Rb/Ba)_{PM}$, low P_2O_5/K_2O and enrichment in light REE, U and Th.

According to Sr-Nd isotope mixing models, the estimated degrees of assimilation of felsic crustal rocks range from about 5–10% (most contaminated Urubici dykes) to 15% (Pitanga dykes), which are in agreement with the mixing results based on Nd and Pb isotopes (Figs. 10 and 12). For modelling, the Paulo Lopes and Garopaba granites (Florisbal et al., 2009) were used as contaminants, whereas the sample FL-98 (MgO ~ 5 wt%; Rocha-Júnior et al., 2012) was chosen as the uncontaminated parental magma of the high-Ti dykes of Urubici type from the FDS, which based on its osmium isotope composition ($\gamma^{187}Os_i = +0.15$) was unquestionably not affected by crustal contamination. According to Shirey and Walker (1998), the osmium isotope composition is a sensitive tracer of crustal contamination, because of the huge contrast between chondritic mantle ($^{187}Os/^{188}Os$ ~ 0.127) and the highly radiogenic continental crust ($^{187}Os/^{188}Os$ ~ 1.7).

Considering that the basaltic trachyandesites have the highest Sr and Pb isotope ratios of all high-Ti analyzed dykes, the required assimilation of felsic rocks would be even higher than that observed on the Pitanga dykes (Figs. 10, 12 and 13). It is important to mention that Florisbal et al. (2009) also report such radiogenic isotope compositions for a dyke from a FDS outcrop nearby Silveira area.

The Pb isotope compositions of the Pitanga and basaltic trachyandesite dykes as well as some the Urubici ones are very radiogenic in comparison to the high-Ti flows from the PMP (Peate et al., 1999; Marques et al., 1999; Rocha-Júnior et al., 2012, 2013) and corroborate crustal contamination in their genesis. The observed arrays in $^{207}Pb/^{204}Pb_m$ and $^{208}Pb/^{204}Pb_m$ versus $^{206}Pb/^{204}Pb_m$ are broadly compatible with the involvement of Paulo Lopes granites (Fig. 11), although a better fit would be attained if the felsic endmember had lower $^{207}Pb/^{204}Pb$ and $^{208}Pb/^{204}Pb$ with respect to $^{206}Pb/^{204}Pb$. According to mixing modelling and considering the sample FL-98 and the Paulo Lopes granites as endmembers, large extents of contamination (up to 30%) would be required to account for the Pb isotope data, since the most radiogenic isotope compositions of the high-Ti dykes are similar to those of the granites.

The differences in the assimilation degrees obtained in the Sr, Nd and Pb isotope modelling, in conjunction with major and trace element behavior, especially in the Pitanga and basaltic trachyandesite dykes, raise some possibilities to explain their genesis, which are not mutually exclusive. In one of them, the assimilated material had isotope compositions other than those of Paulo Lopes granites and Garopaba granitoids, whereas in the other one there was selective crustal Sr, Nd and Pb contamination.

Regarding the last possibility, the FDS emplacement induced local melting of crustal rocks, as verified in the contacts between the dykes and the basement. The original magmas became subject to crustal contamination, which is a complex process since it may involve more than one crustal contaminant and can also generate selective contamination effects (Watson, 1982). According to experimental data (Patiño Douce and Beard, 1995; Patiño Douce, 1999) the partial melting of crustal rocks starts with the breakdown of biotite, followed by the alkali feldspar and quartz, generating selective contamination of the magmas that were in contact with the host rocks. This process may be more meaningful in K-feldspar to modify the Sr isotope compositions of the magmas, since this mineral have multiple, low closure temperatures, ranging from about 150 °C to 300 °C. As the ionic radius of Rb^+ is similar to that of K^+, the K-feldspar minerals acquire high Rb/Sr ratio and become, over time, radiogenic in $^{87}Sr/^{86}Sr$ (Watson, 1982). In addition, preferential incorporation of radiogenic Pb from accessory phases (e.g., zircon, apatite) and/or loosely-bound Pb in mineral surfaces of the host rock submitted to disequilibrium melting due to mafic dyke emplacement are also reported by Waight and Lesher (2010). Therefore, the increase in K, Rb and Ba concentrations, as well as in the Sr and Pb isotope compositions of some samples of this study (especially in the Pitanga and basaltic trachyandesite dykes) may be attributed to the breakdown of biotite and to selective melting of K-feldspar, making it difficult to quantify the crustal fraction assimilated by the magmas during their passage through the crust.

The tectonic aspects related to the FDS were already discussed in previous studies. As mentioned before, Raposo et al. (1998) concluded that these dykes were emplaced after the main phase of the PMP volcanic activity and related to the lithospheric extension due to the opening of the South Atlantic Ocean. On the other hand, Florisbal et al. (2014) proposed that the dykes were the feeders of the Urubici flows. This last interpretation is difficult to reconcile with the fact that the Urubici flood basalts did not suffer contamination by the continental crust, in contrast to the observation that most of the high-Ti dykes show substantial interaction with the granitic host rocks.

Field observations along with the elemental and isotope data of FDS point to dyke emplacement processes other than those of the Urubici basalt feeders. It is important to mention that Caminha-Maciel et al. (2017), using magnetic ground survey on the Central East area of the Santa Catarina Island, showed that the dykes are truncated and probably not deep, intruding in shallow levels. Therefore, at least some of the dykes did not act as large conduits that transported considerable amounts of magma to the surface. In this case, the magmas intruded slowly in weakness zones of the host rocks, significantly interacting with them before the solidification.

6.3. Mantle sources of the high-Ti dykes

The geochemical features of previously published high-Ti basalts of Urubici type from PMP (e.g., Piccirillo and Melfi, 1988; Peate, 1997; Marques et al., 1999, 2016; Peate et al., 1999) and the high-Ti dykes from FDS provide some constraints on the compositions of their parental magmas. The elemental and isotope similarities between basalts and dykes of Urubici type that did not suffer crustal contamination ($^{87}Sr/^{86}Sr_i < 0.7060$) are particularly evident in Figs. 9, 10, 11 and 12 and justify their classification as originated by common mantle sources. Some studies (e.g., Piccirillo and Melfi, 1988; Peate, 1997; Marques et al., 1999, 2016; Peate et al., 1999) have shown that the enriched Sr, Nd and Pb isotope and incompatible element signatures of the Urubici magmas are indicative of a long-term enriched mantle source, such as the Enriched Mantle I (EMI) component, whose elemental and isotope signatures are also present in the both Early and Late Cretaceous carbonatite-alkaline rocks bordering the PMP (e.g., Bizzi et al., 1995; Comin-Chiaramonti and Gomes, 2005). Likewise, this mantle component is recognized in some rocks of the Walvis Ridge and Rio Grande Rise (Hart, 1984; Zindler and Hart, 1986) that led to interpretation that it could represent a subcontinental lithospheric mantle fragment, which was probably left behind during the continental breakup.

In order to explain the characteristics of the Urubici magmas, a petrogenetic model similar to that proposed by Rocha-Júnior et al. (2012, 2013) and Marques et al. (2016) may also be applied. According to these authors, exclusive melting of either ancient SCLM or Tristan da Cunha mantle plume cannot satisfactorily explain the elemental and isotope (Sr, Nd, Pb and Os) features of the PMP rocks. Consequently, to characterize the mantle sources involved in the genesis of the basalt flows and uncontaminated high-Ti Urubici dykes, and account for the chemical and isotope observations, the involvement of asthenospheric mantle is required, which was enriched by fluids and/or magmas related to the Neoproterozoic or even older subduction processes. It is worth noting that this sublithospheric metasomatized mantle source was frozen and coupled to the base of the heterogeneous lithosphere under the Paraná basin. Such a hybridized source (refertilization process) is consistent with other geochemical and geophysical features of the PMP.

For example, the refertilization process has been recently examined by Chaves et al. (2016), based on density and P-wave velocity perturbations in the mantle beneath the south-eastern South America plate. According to those authors, the lithosphere underneath the PMP has a high-density root, indicating that the densification in the mantle and PMP basalt genesis can be related to mantle refertilization, since metasomatic processes (e.g., pyroxenites, eclogites, carbonatites) change the chemical composition and increase the density of the SCLM. Additionally, Padilha et al. (2015) imaged the lithosphere beneath the Paraná Basin, based on electromagnetic induction soundings, and verified that it has a low-resistivity (<500 Ωm). This electromagnetic signature is also a typical characteristic of an altered lithosphere (fertile mantle) due to metasomatic processes (refertilization).

Experimental petrology has shown that pyroxenite or eclogite are important components in the mantle sources of some ocean island basalts and flood basalts (Yaxley and Green, 1998; Yaxley, 2000). In addition, according to Sobolev et al. (2005, 2007), pyroxenite and/or eclogite may be generated by peridotite mantle hybridization with recycled components. These studies indicate that refertilization is a viable process to explain the SCLM underneath the PMP, due to subduction processes that resulted in the western Gondwana assembly, during the Neoproterozoic (Comin-Chiaramonti et al., 1997, 2014). As pointed out by Carlson et al. (2007), the SCLM refertilization process is supported by Goiás Alkaline Province (GAP) xenoliths, which have major and trace element compositions similar to the modern fertile mantle. The GAP is located on the northern margin of the Paraná basin (South of São Francisco Craton), whose underlying mantle underwent several subduction events during the Neoproterozoic.

The results of the mixing calculations are shown in the Figs. 10, 11 and 12. The best-fit in terms of Sr, Nd and Pb isotope compositions is attained through the partial melting of a depleted sublithospheric mantle, represented by an asthenospheric component (DMM), which was hybridized by addition of pyroxenite (<5% in the mixing) and carbonatite (up to 2% in the mixing) melts. The first one is assumed as the same hypothetical "mafic vein" material (pyroxenite EN89-2; Carlson and Irving, 1994; Chesley et al., 2004), while the latter is represented by Jacupiranga and Anitápolis carbonatites (Toyoda et al., 1994; Huang et al., 1995, De Min et al., 2018). The Sr, Nd and Pb concentrations and isotope compositions of the components used in the mixing calculations are shown in Table 2.

In summary, the presence of metasomatic fluids (pyroxenite and carbonatite) in the Paraná SCLM may have promoted the increase of mantle density and the lowering of melting temperature. This refertilized SCLM was melted during Early Cretaceous to produce a voluminous magmatism in Brazil and Namibia, before the southern Atlantic opening, giving rise to the Paraná-Etendeka magmatic province (e.g., Rosset et al., 2007; Rocha-Júnior et al., 2012, 2013; Chaves et al., 2016; Marques et al., 2016).

Plots of Nd isotopes versus Sr and Pb isotope compositions are generally scattered for some FDS rocks, especially for rocks presenting very radiogenic Sr and Pb ($^{87}Sr/^{86}Sr_i > 0.7060$; $^{206}Pb/^{204}Pb_m > 17.85$) isotope compositions, indicative of crustal contamination. It is also observed for samples with lower $^{206}Pb/^{204}Pb_m$ (<17.85), a negative correlation between $^{206}Pb/^{204}Pb_m$ and $^{143}Nd/^{144}Nd_i$, suggesting a low-$^{206}Pb/^{204}Pb$ component similar to the source of group II kimberlites (Smith, 1983) for which an ancient SCLM (purple solid star on Fig. 12) is favored. It is worth emphasizing that the proposed ancient SCLM component is also supported by the model of Chaves et al. (2016), since the lithospheric density underneath the PMP is higher in the north than in the south at a depth of 250–300 km. The slight variation in the SCLM density may indicate that in the southern PMP may have ancient lithospheric fragments, as also evidenced by the Nd model ages (1.1–1.3 Ga) of the basalts from the PMP (e.g., Piccirillo and Melfi, 1988; Comin-Chiaramonti et al., 1997; Peate, 1997; Peate et al., 1999). Another aspect that deserves to

Table 2
Sr, Nd and Pb isotope data and corresponding concentrations of different components used for petrogenetic modelling of the Florianópolis Dyke Swarm mantle sources.

Variable	Sr (μg/g)	$^{87}Sr/^{86}Sr$	Nd (μg/g)	$^{143}Nd/^{144}Nd$	Pb (μg/g)	$^{206}Pb/^{204}Pb$
FL-98[a]	706	0.704704	44.3	0.512419	6.7	17.909
DMM[b]	7.66	0.7025	0.581	0.5134	0.018	17.375
Pyroxenite EN89-2[c]	30	0.70915	10	0.51087	10	19.439
Carbonatite (melt)[d]	10,000	0.70510	80	0.51253	600	17.516
SCLM ancient (melt)[e]	817	0.7075	45	0.5120	32	17.50

[a] Rocha-Júnior et al. (2012).
[b] Workman and Hart (2005), Handler et al. (2005) and GERM data base (http://earthref.org/GERM/).
[c] Carlson and Irving (1994) and Chesley et al. (2004).
[d] Jacupiranga and Anitápolis carbonatites were compiled from Toyoda et al. (1994) and Huang et al. (1995).
[e] SCLM ancient melt were compiled from McDonough (1990) and Pearson et al. (2014), assuming partial melting <6%.

be mentioned is that there are compositional differences between the Archean and post-Archean SCLM (Pearson et al., 2014).

In this context, in order to evaluate the assimilation of even small amounts of ancient lithosphere in the genesis of the Urubici dykes, it was necessary to define the composition of the parental magma before ancient lithospheric interaction or crustal contamination. For such modelling, the sample FL-98 ($\gamma^{187}Os_i = +0.15$) was used again as the parental magma. Note that this initial $\gamma^{187}Os$ is inconsistent with appreciable ancient lithospheric mantle contamination, since ancient SCLM xenoliths are characterized by non-radiogenic osmium isotope compositions ($\gamma^{187}Os \ll 0$; Pearson and Nowell, 2002).

Mixing calculations between the parental magma and SCLM melts are shown in Figs. 10, 11 and 12. The elemental and isotope composition of the low-degree melt of ancient SCLM (Table 2) were compiled from McDonough (1990) and Pearson et al. (2014). Modelling calculations are broadly consistent with large proportions (up to 30%) of ancient lithospheric component inferred from Sr-Nd-Pb isotope and elemental data for the tholeiites with $^{206}Pb/^{204}Pb_m < 17.85$. In addition, if the Urubici flows of the PMP are also considered, the participation of approximately 50% of ancient SCLM would be required. This result apparently also support the idea that the lateral heterogeneity of the continental lithospheric mantle had a crucial role in the petrogenesis of the PMP.

In this view, the Sr, Nd and Pb isotope compositions of the high-Ti PMP basalts reflect the participation of a heterogeneous metasomatized SCLM. In case of Urubici magmas, it seems that there was a prevalent participation of Archean SCLM, whereas for the Pitanga ones there was involvement of Neoproterozoic SCLM. Melting of fragments of ancient SCLM left behind during the Western Gondwana rupture (e.g., Smith and Lewis, 1999; Comin-Chiaramonti and Gomes, 2005), as well as small-scale mantle convection at SCLM edge (e.g., King and Anderson, 1998; Ernesto et al., 2002) and/or thermal erosion of its base (e.g., Class and Roex, 2006; Meyzen et al., 2007) are possible alternatives to account for the isotope signature of Walvis Ridge and Rio Grande Rise basalts, no requiring to invoke a mantle plume to explain their genesis as recently proposed by Hoernle et al. (2015).

It is also important to note that according to the model proposed by the last authors, it would be expected that the osmium isotope signature of Tristan mantle plume have a depleted composition, similar to that derived from the modern mantle such as abyssal peridotites and chromites from ophiolites, whose $^{187}Os/^{188}Os$ composition varies from 0.122 to 0.132 (Snow and Reisberg, 1995; Walker et al., 2002). However, Rocha-Júnior et al. (2012) show that the osmium isotope signature of Tristan basalts is extremely radiogenic in ^{187}Os (initial $\gamma^{187}Os$ values range from +15 to +80), requiring mechanisms other them that those proposed by Hoernle et al. (2015) for their genesis.

Moreover, Baba et al. (2016), based on marine magnetotelluric and seismological surveys (conducted in 2012–2013), imaged the three-dimensional structure of the upper mantle adjacent to Tristan da Cunha island. These researchers found that the 3-D electrical conductivity of the region does not support the idea of a vertical conductor (such as a mantle plume) rising from the core-mantle boundary or the 670 km seismic discontinuity beneath the Tristan da Cunha island.

7. Concluding remarks

The main results of the present study are summarized below:

1. The Florianópolis Dyke Swarm, associated with the Paraná Magmatic Province (PMP), is located at Santa Catarina Island and adjacent continental area (southern Brazil). In the Santa Catarina Island, the dykes are 0.1 to 70 m thick and preferably oriented in two directions. About 80% of the dykes trend N30°E–N55°E, coinciding with the orientation of the host rocks from the Dom Feliciano Belt. The N15°W–N45°W striking is subordinate.
2. Most of the dykes are tholeiites and have SiO_2 contents ranging from 50 wt% to 55 wt%. The vast majority of the intrusions presents high-Ti (TiO_2 > 3 wt%) contents, although some dykes of low-Ti (TiO_2 < 2 wt%) type are also found. Crosscutting relationships indicate that some low-Ti dykes (NW trending) are younger than the high-Ti ones (NE trending).
3. The high-Ti dykes containing Sr > 550 μg/g are by far the dominant type, showing geochemical characteristics similar to those of the Urubici flows from the PMP. Subordinate high-Ti dykes containing Sr < 550 μg/g occur and are similar to the Pitanga flows. A scarce number of high-Ti dykes have a slight alkaline tendency and classify as basaltic trachyandesites, presenting geochemical features resembling those of the Urubici dykes.
4. The low-Ti dykes are few and show a significant compositional variability (SiO_2: 50.4–64.5 wt%), which is compatible with an evolution by fractional crystallization, mainly controlled by clinopyroxene, plagioclase and magnetite, concurrent with crustal contamination processes, as observed for the volcanic analogues from southern PMP. The most primitive low-Ti dykes have hybrid characteristics of Ribeira and Esmeralda-Gramado magmas, which would be the result of a slight interaction with the Urubici dykes, since all these low-Ti dykes crosscut the high-Ti ones.
5. In contrast with the high-Ti flows from the PMP, a considerable number of high-Ti dykes experienced large extents (at least 15%) of crustal contamination with the felsic host rocks, generating a substantial increase of $(Rb/Ba)_{PM}$ (up to 2.6) and decrease of P_2O_5/K_2O (0.30–0.18) ratios. This process also caused a decrease of TiO_2 and Sr, and generated rocks presenting the observed characteristics of the Pitanga and basaltic trachyandesite dykes with very radiogenic Sr ($^{87}Sr/^{86}Sr_i$ up to 0.71758) and Pb ($^{206}Pb/^{204}Pb_m$ up to 19.441) isotope compositions.
6. The assimilation degrees calculated by the elemental and isotope mixing modelling are not perfectly concordant, suggesting that the contaminant would be other than the Garopaba and Paulo Lopes granites (used as end-members) and/or the contamination was a selective process, as shown by several experimental studies involving re-melting of crustal rocks containing biotite, K-feldspar, zircon and apatite.
7. According to Sr, Nd and Pb isotope modelling, the magmas that generated the uncontaminated high-Ti Urubici dykes were the result of partial melting of a depleted sublithospheric mantle (DMM-type) hybridized by addition of pyroxenite (<5%) and Anitápolis-Jacupiranga carbonatite (<2%) melts. Moreover, the negative correlation between Pb and Nd isotopes compositions observed for the high-Ti dykes and flows of Urubici type points to the involvement of a large proportion (up to 50%) of ancient subcontinental lithospheric mantle (SCLM), not evidenced in the mantle sources of the northern high-Ti Pitanga flows (dominated by Neoproterozoic SCLM). Both refertilized mantle sources and the involvement of an ancient SCLM are corroborated by the results of electromagnetic induction soundings (Padilha et al., 2015), as well as those of density and P-wave velocity perturbations (Chaves et al., 2016) in the mantle beneath the Paraná Basin.

Supplementary data to this article can be found online at http://dx.doi.org/10.1016/j.jvolgeores.2017.07.005.

Acknowledgements

This paper is in honor to Enzo M. Piccirillo, who participated of some field trips to Santa Catarina Island as well as in the first studies about the investigated dykes, and devoted most of his academic career studying the Paraná Magmatic Province. Many thanks are due to Ricardo Petrini, who kindly provided unpublished Sr and Nd isotope data in a considerable number of samples of the studied dykes. We are grateful to Piero Comin-Chiaramonti by very fruitful discussions about the Paraná magmatism and comments in early versions of the manuscript. The geophysicist Leandro Gabioli is also acknowledged for some analyses of

trace elements using neutron activation method. This paper benefited from suggestions of an anonymous reviewer and Peter Schaff, who was very kind, also improving the English grammar. This research was supported by the Fundação de Amparo à Pesquisa do Estado de São Paulo (FAPESP; Procs. 2004/10081-9, 2012/06082-6). L.S.M., M.B. and A.M.G.F. are CNPq Fellow Researchers.

References

Almeida, F.F.M., 1986. Distribuição regional e relações tectônicas do magmatismo pós-paleozoico no Brasil. Rev. Bras. Geoci. 16 (4), 325–349.

Anderson, D.L., 1994. Superplumes or supercontinents? Geology 22, 39–42.

Anderson, D.L., 2005. Large igneous provinces, delamination, and fertile mantle. Elements 1, 271–275.

Baba, K., Chen, J., Sommer, M., Utada, H., Geissler, W.H., Jokat, W., Jegen, M., 2016. Marine magnetotellurics imaged no distinct plume beneath the Tristan da Cunha hotspot in the southern Atlantic Ocean. Tectonophysics. http://dx.doi.org/10.1016/j.tecto.2016.09.033.

Babinski, M., Van Schmus, W.R., Chemale Jr., F., 1999. Pb-Pb dating and Pb isotope geochemistry of Neoproterozoic carbonate rocks from the São Francisco basin, Brazil: implications for the mobility of Pb isotopes during tectonism and metamorphism. Chem. Geol. 160, 175–199.

Barreto, C.J.S., Lafon, J.M., Lima, E.F., Sommer, C.A., 2016. Geochemical and Sr-Nd-Pb isotopic insight into the low-Ti basalts from southern Paraná Igneous Province, Brazil: the role of crustal contamination. Int. Geol. Rev. 58, 1–26.

Bellieni, G., Comin-Chiaramonti, P., Marques, L.S., Melfi, A.J., Piccirillo, E.M., Nardy, A.J.R., Roisenberg, A., 1984a. High- and low-Ti flood basalts from the Paraná plateau (Brazil): petrogenetic and geochemical aspects bearing on their mantle origin. Neues Jb. Mineral. Abh. 150, 273–306.

Bellieni, G., Comin-Chiaramonti, P., Marques, L.S., Melfi, A.J., Piccirillo, E.M., Stolfa, D., 1984b. Low-pressure evolution of basalt sills from bore-holes in the Paraná Basin. Tschermaks Min. Petr. Mitt. 33, 25–47.

Bellieni, G., Comin-Chiaramonti, P., Marques, L.S., Melfi, A.J., Nardy, A.J.R., Papatrechas, C., Piccirillo, E.M., Roisenberg, A., 1986. Petrogenetic aspects of acid and basaltic lavas from the Paraná plateau (Brazil): geological, mineralogical and petrochemical relationships. J. Petrol. 27, 915–944.

Bizzi, L.A., De Wit, M.J., Smith, C.B., McDonald, I., Armstrong, R.A., 1995. Heterogeneous enriched mantle materials and Dupal-type magmatism along the SW margin of the São Francisco Craton, Brazil. J. Geodyn. 20 (4), 469–491.

Bryan, S.E., Ernst, R.E., 2008. Revised definition of Large Igneous Provinces (LIPs). Earth Sci. Rev. 86 (1–4), 175–202.

Caminha-Maciel, G., Ernesto, M., Borges, W.R., Bresolin, J., Lemos, R., 2017. Evaluation of mafic dyke swarm continuity under the Joaquina dune field with ground magnetic survey. Braz. J. Geol. 47 (2), 237–247.

Carlson, R.W., Irving, A.J., 1994. Depletion and enrichment history of subcontinental and lithospheric mantle: an Os, Sr, Nd and Pb isotopic study from the northwestern Wyoming Craton. Earth Planet. Sci. Lett. 126, 457–472.

Carlson, R.W., Araujo, A.L.N., Junqueira-Brod, T.C., 2007. Chemical and isotopic relationships between peridotite xenoliths and mafic-ultrapotassic rocks from Southern Brazil. Chem. Geol. 242, 415–434.

Chaves, C., Ussami, N., Ritsema, J., 2016. Density and P-wave velocity structure beneath the Paraná Magmatic Province: refertilization of an ancient lithospheric mantle. Geochem. Geophys. Geosyst. 17. http://dx.doi.org/10.1002/2016GC006369.

Chesley, J.T., Righter, K., Ruiz, J., 2004. Large-scale mantle metasomatism: a Re/Os perspective. Earth Planet. Sci. Lett. 219 (1–2), 49–60.

Class, C., Roex, A.P., 2006. Continental material in shallow oceanic mantle - how does it get there? Geology 34, 129–132.

Coffin, M.F., Eldholm, O., 1994. Large igneous provinces: crustal structure, dimensions, and external consequences. Rev. Geophys. 32, 1–36.

Coltice, N., Phillips, B.R., Bertrand, H., Ricard, Y., Rey, P., 2007. Global warming of the mantle at the origin of flood basalts over continents. Geology 35 (5), 391–394.

Comin-Chiaramonti, P., Gomes, C.B. (Eds.), 2005. Mesozoic to Cenozoic Alkaline Magmatism in the Brazilian Platform. EDUSP/FAPESP, São Paulo, Brazil (750 pp.).

Comin-Chiaramonti, P., Cundari, A., Piccirillo, E.M., Gomes, C.B., Castorina, F., Censi, P., De Min, A., Marzoli, A., Speziale, S., Velázquez, V.F., 1997. Potassic and sodic igneous rocks from Eastern Paraguay: their origin from the lithospheric mantle and genetic relationships with associated Paraná food tholeiites. J. Petrol. 38 (4), 495–528.

Comin-Chiaramonti, P., De Min, A., Girardi, A.V., Gomes, C.B., 2014. Carbonatites and primary carbonates in the Rio Apa and Amambay regions, NE Paraguay. Lithos 188, 84–96.

CPRM, 2014. Serviço Geológico do Brasil. Mapa geológico do Estado de Santa Catarina – Escala 1:500.000 (September, 1st).

De Min, A., Piccirillo, E.M., Marzoli, A., Bellieni, G., Renne, P.R., Ernesto, M., Marques, L.S., 2003. The Central Atlantic Magmatic Province (CAMP) in Brazil: petrology, geochemistry, $^{40}Ar/^{39}Ar$ ages, paleomagnetism and geodynamic implications. In: Hames, W., McHone, J.G., Renne, P.R., Ruppel, C. (Eds.), The Central Atlantic Magmatic Province. AGU Geophysical Monograph 136, pp. 91–128.

De Min, A., Callegaro, S., Marzoli, A., Nardy, A.J.R., Chiaradia, M., Marques, L.S., Gabbarrini, I., 2018. Stratigraphy of four lava sequences from central-south Paraná basin and petrogenetic implications. J. Volcanol. Geotherm. Res. 355, 232–252.

Déckart, K., Féraud, G., Marques, L.S., Bertrand, H., 1998. New time constraints on dyke swarms related to the Paraná-Etendeka magmatic province, and subsequent South Atlantic opening, southeastern Brazil. J. Volcanol. Geotherm. Res. 80, 67–83.

Ernesto, M., Raposo, M.I.B., Marques, L.S., Renne, P.R., Diogo, L.A., De Min, A., 1999. Paleomagnetism, geochemistry and $^{40}Ar/^{39}Ar$ dating of the North-eastern Paraná magmatic province: tectonic implications. J. Geodyn. 28, 321–340.

Ernesto, M., Marques, L.S., Piccirillo, E.M., Molina, E.C., Ussami, N., Comin-Chiaramonti, P., Bellieni, G., 2002. Paraná Magmatic Province - Tristan da Cunha plume system: fixed versus mobile plume, petrogenetic considerations and alternative heat sources. J. Volcanol. Geotherm. Res. 118, 15–36.

Ernst, R.E., 2014. Large Igneous Provinces. Cambridge University Press (653 pp.).

Ewart, A., Marsh, J.S., Milner, S.C., Duncan, A.R., Kamber, B.S., Armstrong, R.A., 2004. Petrology and geochemistry of Early Cretaceous bimodal continental volcanism of the NW Etendeka, Namibia. Part 1: introduction, mafic lavas and re-evaluation of mantle source components. J. Petrol. 45, 59–105.

Figueiredo, A.M.G., Marques, L.S., 1989. Determination of rare earths and other trace elements in the Brazilian geological standards BB-1 and GB-1 by neutron activation analysis. Geochim. Bras. 3, 1–8.

Florisbal, L.M., Bitencourt, M.F., Nardi, L.V.S., Conceição, R.V., 2009. Early post-collisional granitic and coeval mafic magmatism of medium- to high-K tholeiitic affinity within the Neoproterozoic Southern Brazilian Shear Belt. Precambrian Res. 175, 135–148.

Florisbal, L.M., Heaman, L.M., Janasi, V.A., Bitencourt, M.F., 2014. Tectonic significance of the Florianópolis Dyke Swarm, Paraná-Etendeka Magmatic Province: a reappraisal based on precise U-Pb dating. J. Volcanol. Geotherm. Res. 289, 140–150.

Garda, G.M., Schorscher, J.H.D., 1996. Os diques costeiros básicos e ultrabásicos adjacentes ao Canal de São Sebastião (litoral norte do Estado de São Paulo). Rev. Inst. Geol. 17 (1/2), 7–31.

Garland, F., Hawkesworth, C.J., Mantovani, M.S.M., 1995. Description and petrogenesis of the Paraná rzhyolites, Southern Brazil. J. Petrol. 36, 1193–1227.

Gibson, S.A., Thompson, R.N., Leonardos, O.H., Dickin, A.P., Mitchell, J.G., 1999. The limited extent of plume-lithosphere interactions during continental flood-basalt genesis: geochemical evidence from Cretaceous magmatism in southern Brazil. Contrib. Mineral. Petrol. 137, 147–169.

Guedes, E., Heilbron, M., Vasconcelos, P., Valeriano, C.M., Almeida, J.C.H., Teixeira, W., Thomaz Filho, A., 2005. K-Ar and Ar-Ar ages of dikes emplaced in the onshore basement of Santos Basin, Resende Area, SE, Brazil: implications for the South Atlantic opening and a Tertiary reactivation. J. S. Am. Earth Sci. 18, 145–178.

Guedes, E., Heilbron, M., Valeriano, C.M., Almeida, J.C.H., Szatmari, P., 2016. Evidence of Gondwana early rifting process recorded by Resende-Ilha Grande Dike Swarm, southern Rio de Janeiro, Brazil. J. S. Am. Earth Sci. 67, 11–24.

Handler, M.R., Bennett, V.C., Carlson, R.W., 2005. Nd, Sr and Os isotope systematics in young, fertile spinel peridotite xenoliths from northern Queensland, Australia: a unique view of depleted MORB mantle? Geochim. Cosmochim. Acta 69 (24), 5747–5763.

Hart, S.R., 1984. A large-scale isotope anomaly in the southern hemisphere mantle. Nature 309, 753–757.

Hawkesworth, C.J., Mantovani, M.S.M., Taylor, P.N., Palacz, Z., 1986. Evidence from the Paraná of south Brazil for a continental contribution to Dupal basalts. Nature 322, 356–359.

He, C., Santosh, M., Wu, J., Chen, X., 2014. Plume or no plume: Emeishan Large Igneous Province in southwest China revisited from receiver function analysis. Physi. Planet. Inter. 232, 72–78.

Hoernle, K., Rohde, J., Hauff, F., Garbe-Schonberg, D., Homrighausen, S., Werner, R., Morgan, J.P., 2015. How and when plume zonation appeared during the 132 Myr evolution of the Tristan Hotspot. Nat. Commun. http://dx.doi.org/10.1038/ncomms8799.

Huang, Y.-M., Hawkesworth, C.J., van Calsteren, P., McDermott, F., 1995. Geochemical characteristics and origin of the Jacupiranga carbonatites, Brazil. Chem. Geol. 119, 79–99.

Iacumin, M., De Min, A., Piccirillo, E.M., Bellieni, G., 2003. Source mantle heterogeneity and its role in the genesis of Late Archean-Proterozoic (2.7-1.0 Ga) and Mesozoic (200 and 130 Ma) tholeiitic magmatism in the South American Platform. Earth-Sci. Rev. 62, 365–397.

Irvine, T.N., Baragar, W.R.A., 1971. A guide to the chemical classification of the common volcanic rocks. Can. J. Earth Sci. 8, 523–548.

King, S.D., Anderson, D.L., 1998. Edge-driven convection. Earth Planet. Sci. Lett. 160, 289–296.

Le Bas, M.J., Le Maitre, R.W., Streckeisen, A., Zanettin, B., 1986. A chemical classification of volcanic rocks based on the total alkali-silica diagram. J. Petrol. 27, 745–750.

Lustrino, M., 2005. How the delamination and detachment of lower crust can influence basaltic magmatism. Earth-Sci. Rev. 72, 21–38.

Machado, F.B., Nardy, A.J.R., Oliveira, M.A.F., 2007. Geologia e aspectos petrológicos das rochas intrusivas e efusivas mesozoicas de parte da borda leste da Bacia do Paraná no estado de São Paulo. Rev. Bras. Geoci. 37 (1), 64–80.

Machado, F.B., Rocha-Júnior, E.R.V., Marques, L.S., Nardy, A.J.R., 2015. Volcanological aspects of the northwest region of Paraná continental flood basalts (Brazil). Solid Earth 6, 227–241.

Maniesi, V., Oliveira, M.A.F., 1997. Petrologia das soleiras de diabásio de Reserva e Salto do Itararé, PR. Geochim. Bras. 11, 153–169.

Mantovani, M.S.M., Marques, L.S., Sousa, M.A., Atalla, L.T., Civetta, L., Innocenti, F., 1985. Trace element and strontium isotope constraints on the origin and evolution of Paraná continental flood basalts of Santa Catarina State (southern Brazil). J. Petrol. 26, 187–209.

Marques, L.S., 2001. Geoquímica dos diques toleíticos da costa sul-sudeste do Brasil: contribuição ao conhecimento da Província Magmática do Paraná. IAG, Universidade de São Paulo, São Paulo, Tese de Livre Docência (86 pp.).

Marques, L.S., Ernesto, M., 2004. O magmatismo toleítico da Bacia do Paraná. In: Mantesso Neto, V., Bartorelli, A., Carneiro, C.R., Brito Neves, B.B. (Eds.), Geologia do Continente Sul-Americano: Evolução da obra de Fernando Flávio Marques de Almeida. Beca Produções Culturais Ltda., São Paulo, pp. 245–263.

Marques, L.S., Piccirillo, E.M., Melfi, A.J., Comin-Chiaramonti, P., Bellieni, G., 1989. Distribuição de terras raras e outros elementos traços em basaltos da Bacia do Paraná (Brasil Meridional). Geochim. Bras. 3, 33–50.

Marques, L.S., Dupré, B., Piccirillo, E.M., 1999. Mantle source compositions of the Paraná Magmatic Province: evidence from trace element and Sr - Nd - Pb isotope geochemistry. J. Geodyn. 28, 439–459.

Marques, L.S., Rocha-Júnior, E.R.V., Babinski, M., Carvas, K.Z., Petronilho, L.A., De Min, A., 2016. Lead isotope constraints on the mantle sources involved in the genesis of Mesozoic high-Ti tholeiite dykes (Urubici type) from the São Francisco Craton (Southern Espinhaço, Brazil). Braz. J. Geol. 46 (1), 105–122.

McDonough, W.F., 1990. Constraints on the composition of the continental lithospheric mantle. Earth Planet. Sci. Lett. 101, 1–18.

McDonough, W.F., Sun, S.-S., 1995. The composition of the Earth. Chem. Geol. 120, 223–253.

Merle, R., Marzoli, A., Bertrand, H., Reisberg, L., Verati, C., Zimmermann, C., Chiaradia, M., Bellieni, G., Ernesto, M., 2011. $^{40}Ar/^{39}Ar$ ages and Sr-Nd-Pb-Os geochemistry of CAMP tholeiites from Western Maranhão basin (NE Brazil). Lithos 122, 137–151.

Meyzen, C.M., Blichert-Toft, J., Ludden, J.N., Humler, E., Mével, C., Albarède, F., 2007. Isotopic portrayal of Earth's upper mantle flow field. Nature 447, 1069–1074.

Milner, S., le Roex, A.P., 1996. Isotope characteristics of the Okenyenya igneous complex, northern Namibia: constraints on the composition of the early Tristan Plume and the origin of the EM1 mantle component. Earth Planet. Sci. Lett. 141, 277–291.

Nardy, A.J.R., Machado, F.B., Oliveira, M.A.F., 2008. As rochas vulcânicas mesozoicas ácidas da Bacia do Paraná: litoestratigrafia e considerações geoquímico-estratigráficas. Rev. Bras. Geoci. 38 (1), 178–195.

Padilha, A.L., Vitorello, I., Antunes, C.E., Pádua, M.B., 2015. Imaging three-dimensional crustal conductivity structures reflecting continental flood basalt effects hidden beneath thick intracratonic sedimentary basin. J. Geophys. Res. Solid Earth 120, 4702–4719.

Patiño Douce, A.E., 1999. What do experiments tell us about the relative contributions of crust and mantle to the origin of granitic magmas? In: Castro, A., Fernandez, C., Vigneresse, J.L. (Eds.), Understanding Granites. Integrating New and Classical Techniques. Geological Society, London, Special Publications 158, pp. 55–75

Patiño Douce, A.E., Beard, J.S., 1995. Dehydration-melting of biotite gneiss and quartz amphibolite from 3 to 15 kbar. J. Petrol. 36, 707–738.

Pearson, D.G., Nowell, G.M., 2002. The continental lithospheric mantle: characteristics and significance as a mantle reservoir. Philos. Transact. A Math. Phys. Eng. Sci. 360, 2383–2410.

Pearson, D.G., Canil, D., Shirey, S.B., 2014. Mantle samples included in volcanic rocks: xenoliths and diamonds. In: Holland, H., Turekian, K. (Eds.), Treatise on Geochemistry, 2nd edition Elsevier, Amsterdam, pp. 169–253.

Peate, D.W., 1997. The Paraná - Etendeka Province. In: Mahoney, J.J., Coffin, M.F. (Eds.), Large Igneous Provinces: Continental, Oceanic, and Planetary Flood Volcanism. AGU Geophysical Monograph vol. 100, pp. 217–245.

Peate, P.W., Hawkesworth, C.J., 1996. Lithospheric to asthenospheric transition in low-Ti flood basalts from southern Paraná: Brazil. Chem. Geol. 127, 1–24.

Peate, D.W., Hawkesworth, C.J., Mantovani, M.S.M., 1992. Chemical stratigraphy of the Paraná lavas (South America): classification of magma types and their spatial distribution. Bull. Volcanol. 55, 119–139.

Peate, D.W., Hawkesworth, C.J., Mantovani, M.S.M., Rogers, N.W., Turner, S.P., 1999. Petrogenesis and stratigraphy of the high Ti/Y Urubici magma type in the Paraná flood basalt province and implications for the nature of "Dupal"-type mantle in the South American region. J. Petrol. 40, 451–473.

Petrini, R., Civetta, L., Piccirillo, E.M., Bellieni, G., Comin-Chiaramonti, P., Marques, L.S., Melfi, A.J., 1987. Mantle heterogeneity and crustal contamination in the genesis of low-Ti continental flood basalts from the Paraná plateau (Brazil): Sr-Nd isotope and geochemical evidence. J. Petrol. 28, 701–726.

Piccirillo, E.M., Melfi, A.J. (Eds.), 1988. The Mesozoic flood volcanism of the Paraná Basin: petrogenetic and geophysical aspects. São Paulo, Instituto Astronômico e Geofísico. Universidade de São Paulo, São Paulo, Brazil 600 p.

Piccirillo, E.M., Melfi, A.J., Comin-Chiaramonti, P., Bellieni, G., Ernesto, M., Marques, L.S., Nardy, A.J.R., Pacca, I.G., Roisenberg, A., Stolfa, D., 1988. Continental Flood Volcanism from the Paraná Basin (Brazil). In: Macdougall, J.D. (Ed.) Continental Flood Basalts. Kluwer Academic Publishers, Dordrecht, pp. 195–238.

Piccirillo, E.M., Raposo, M.I.B., Melfi, A.J., Comin-Chiaramonti, P., Bellieni, G., Cordani, U.G., Kawashita, K., 1987. Bimodal fissural volcanic suites from the Paraná Basin (Brazil): K-Ar age, Sr-isotopes and geochemistry. Geochim. Bras. 1, 53–69.

Piccirillo, E.M., Civetta, L., Petrini, R., Longinelli, A., Bellieni, G., Comin-Chiaramonti, P., Marques, L.S., Melfi, A.J., 1989. Regional variations within the Paraná flood basalts (southern Brazil): evidence for subcontinental mantle heterogeneity and crustal contamination. Chem. Geol. 75, 103–122.

Piccirillo, E.M., Bellieni, G., Cavazzini, G., Comin-Chiaramonti, P., Petrini, R., Melfi, A.J., Pinese, J.P.P., Zantadeschi, P., De Min, A., 1990. Lower cretaceous tholeiitic dyke swarms from the Ponta Grossa Arch (southeast Brazil): petrology, Sr-Nd isotopes and genetic relationships with the Paraná flood volcanics. Chem. Geol. 89, 19–48.

Raposo, M.I.B., Ernesto, M., Renne, P.R., 1998. Paleomagnetism and $^{40}Ar/^{39}Ar$ dating of the Early Cretaceous Florianópolis dike swarm (Santa Catarina Island), Southern Brazil. Phys. Earth Planet. Inter. 108, 275–290.

Renne, P.R., Ernesto, M., Pacca, I.G., Coe, R.S., Glen, J., Prevot, M., Perrin, M., 1992. Rapid eruption of the Paraná flood volcanics, rifting of Gondwanaland and the Cretaceous boundary. Science 258, 975–979.

Renne, P.R., Mertz, D.F., Ernesto, M., Marques, L.S., Teixeira, W., Ens, H.H., Richards, M.A., 1993. Geochronologic constrains on magmatic and tectonic evolution of the Paraná Province. EOS Am. Geophys. Union 26, 553.

Renne, P.R., Déckart, K., Ernesto, M., Féraud, G., Piccirillo, E.M., 1996. Age of the Ponta Grossa dyke swarm (Brazil), and implications to Paraná flood volcanism. Earth Planet. Sci. Lett. 144, 199–211.

Renne, P.R., Mundil, R., Balco, G., Min, K., Ludwig, K.R., 2010. Joint determination of ^{40}K decay constants and $^{40}Ar/^{40}K$ for the Fish Canyon sanidine standard, and improved accuracy for $^{40}Ar/^{39}Ar$ geochronology. Geochim. Cosmochim. Acta 74, 5349–5367.

Richards, M.A., Duncan, R.A., Courtillot, V.E., 1989. Flood basalts and hot-spot tracks: plume heads and tails. Science 246, 103–107.

Rocha-Júnior, E.R.V., Puchtel, I.S., Marques, L.S., Walker, R.J., Machado, F.B., Nardy, A.J.R., Babinski, M., Figueiredo, A.M.G., 2012. Re-Os isotope and highly siderophile element systematics of the Paraná Continental Flood Basalts (Brazil). Earth Planet. Sci. Lett. 337–338, 164–173.

Rocha-Júnior, E.R.V., Marques, L.S., Babinski, M., Nardy, A.J.R., Figueiredo, A.M.G., Machado, F.B., 2013. Sr-Nd-Pb isotopic constraints on the nature of the mantle sources involved in the genesis of the high-Ti tholeiites from Northern Paraná Continental Flood Basalts (Brazil). J. S. Am. Earth Sci. 46, 9–25.

Rosset, A., De Min, A., Marques, L.S., Macambira, M.J.B., Ernesto, M., Renne, P.R., Piccirillo, E.M., 2007. Genesis and geodynamic significance of Mesoproterozoic and Early Cretaceous tholeiitic dyke swarms from the São Francisco Craton (Brazil). J. S. Am. Earth Sci. 24, 69–92.

Self, S., Thordarson, T., Keszthelyi, L., 1997. Emplacement of continental flood basalt flows. In: Mahoney, J.J., Coffin, M. (Eds.), Large Igneous Provinces: Continental, Oceanic, and Planetary Flood Volcanism. AGU Geophysical Monograph vol. 100, pp. 381–410.

Shirey, S.B., Walker, R.J., 1998. The Re–Os isotope system in cosmochemistry and high-temperature geochemistry. Annu. Rev. Earth Planet. Sci. 26, 423–500.

Smith, C.B, 1983. Pb, Sr and Nd isotopic evidence for sources of southern African Cretaceous kimberlites. Nature 304, 51–54.

Smith, A.D., Lewis, C., 1999. The planet beyond the plume hypothesis. Earth-Sci. Rev. 48, 135–182.

Snow, J.E., Reisberg, L., 1995. Os isotopic systematics of the MORB mantle: results from altered abyssal peridotites. Earth Planet. Sci. Lett. 133, 411–421.

Sobolev, A.V., Hofmann, A.W., Sobolev, S.V., Nikogosian, I.K., 2005. An olivine-free mantle source of Hawaiian shield basalts. Nature 434, 590–597.

Sobolev, A.V., et al., 2007. The amount of recycled crust in sources of mantle-derived melts. Science 316, 412–417 (19 other authors).

Thiede, D.S., Vasconcelos, P.M., 2010. Paraná flood basalts: rapid extrusion hypothesis confirmed by new $^{40}Ar/^{39}Ar$ results. Geology 38 (8), 747–750.

Toyoda, K., Horiuchi, H., Tokonami, M., 1994. Dupal anomaly of the Brazilian carbonatites: geochemical correlations with hotspots in the South Atlantic and implications for the mantle source. Earth Planet. Sci. Lett. 126, 315–331.

Valente, S.C., Corval, A., Duarte, B.P., Ellam, R.B., Fallick, A.E., Dutra, T., 2007. Tectonic boundaries, crustal weakness zones and plume-subcontinental lithospheric mantle interactions in the Serra do Mar Dyke Swarm, SE Brazil. Rev. Bras. Geoci. 37 (1), 194–201.

Waight, T.E., Lesher, C.E., 2010. Pb isotopes during crustal melting and magma mingling - a cautionary tale from the Miki Fjord macrodike, central east Greenland. Lithos 118, 191–201.

Walker, R.J., Prichard, H.M., Ishiwatari, A., Pimentel, M., 2002. The osmium isotopic composition of convecting upper mantle deduced from ophiolite chromites. Geochim. Cosmochim. Acta 66 (2), 329–345.

Watson, E.B., 1982. Basalt contamination by continental crust: some experiments and models. Contrib. Mineral. Petrol. 80, 73–87.

White, R., McKenzie, D.J., 1989. Magmatism at rift zones: the generation of volcanic continental margins and flood basalts. J. Geophys. Res. 94 (B6), 7685–7729.

Will, T.M., Frimmel, H.E., Pfänder, J.A., 2016. Möwe Bay Dykes, Northwestern Namibia: geochemical and geochronological evidence for different mantle source regions during the Cretaceous opening of the South Atlantic. Chem. Geol. 444, 141–157.

Workman, R.K., Hart, S.R., 2005. Major and trace element composition of the depleted MORB mantle (DMM). Earth Planet. Sci. Lett. 231, 53–72.

Yaxley, G.M., 2000. Experimental study of the phase and melting relations of homogeneous basalt + peridotite mixtures and implications for the petrogenesis of food basalts. Contrib. Mineral. Petrol. 139, 326–338.

Yaxley, G.M., Green, D.H., 1998. Reactions between eclogite and peridotite: Mantle refertilization by subducted oceanic crust: Schweizerische Mineralogische und Petrographische Mitteilungen. 78 pp. 243–255.

Zindler, A., Hart, S.R., 1986. Chemical geodynamics. Annu. Rev. Earth Planet. Sci. 14, 493–571.